

1 **New insight into the spatiotemporal variability and source apportionments of**  
2 **C<sub>1</sub>-C<sub>4</sub> alkyl nitrates in Hong Kong**

3 Z.H. Ling<sup>1,2</sup>, H. Guo<sup>2\*</sup>, I.J. Simpson<sup>3</sup>, S.M. Saunders<sup>4</sup>, S.H.M. Lam<sup>4,5</sup>, X.P. Lyu<sup>2</sup>, D.R.  
4 Blake<sup>3</sup>

5 <sup>1</sup> School of Atmospheric Sciences, Sun Yat-sen University, Guangzhou, China

6 <sup>2</sup> Air Quality Studies, Department of Civil and Environmental Engineering, The Hong  
7 Kong Polytechnic University, Hong Kong

8 <sup>3</sup> Department of Chemistry, University of California at Irvine, California, USA

9 <sup>4</sup> School of Chemistry and Biochemistry, University of Western Australia, Perth,  
10 Western Australia, Australia

11 <sup>5</sup> Pacific Environment Limited, Perth, Western Australia, Australia

12

13 \* Corresponding author. Tel: +852 34003962. Fax: +852 23346389. Email:  
14 [ceguohai@polyu.edu.hk](mailto:ceguohai@polyu.edu.hk)

15

1 **Abstract**

2 C<sub>1</sub>-C<sub>4</sub> alkyl nitrates (RONO<sub>2</sub>) were measured concurrently at a mountain site, *i.e.*, Mt.  
3 Tai Mo Shan (TMS), and an urban site, *i.e.*, Tsuen Wan (TW) at the foot of the same  
4 mountain in Hong Kong from September to November 2010. Although the levels of  
5 parent hydrocarbons were much lower at TMS ( $p < 0.05$ ), similar alkyl nitrate levels  
6 were found at both sites regardless of the elevation difference, suggesting various  
7 source contributions of alkyl nitrates at the two sites. Prior to using a positive matrix  
8 factorization (PMF) model, the data at TW were divided into “meso” and “non-meso”  
9 scenarios for the investigation of source apportionments with the influence of  
10 mesoscale circulation and regional transport, respectively. Secondary formation was  
11 the prominent contributor of alkyl nitrates in the “meso” scenario ( $60 \pm 2\%$ ,  $60.2 \pm$   
12  $1.2$  pptv), followed by biomass burning and oceanic emissions, while biomass burning  
13 and secondary formation made comparable contributions to alkyl nitrates in the  
14 “non-meso” scenario, highlighting the strong emissions of biomass burning in the  
15 inland Pearl River Delta (PRD) region. On the other hand, alkyl nitrates at TMS were  
16 mainly due to the photo-oxidation of parent hydrocarbons at TW when mesoscale  
17 circulation, *i.e.*, valley breezes occurred, contributing 52-86% to the levels of alkyl  
18 nitrates at TMS. In contrast, regional transport from the inland PRD region made  
19 significant contributions to the levels of alkyl nitrates (~58-82%) at TMS in the  
20 “non-meso” scenario, resulting in similar levels of alkyl nitrates observed at the two  
21 sites. The simulation of secondary formation pathways using a photochemical box  
22 model found that the reaction of alkyl peroxy radicals (RO<sub>2</sub>) with nitric oxide (NO)  
23 dominated the formation of RONO<sub>2</sub> at both sites, and the formation of alkyl nitrates  
24 contributed negatively to O<sub>3</sub> production, with average reduction rates of 4.1 and 4.7  
25 pptv/pptv at TMS and TW, respectively.

26

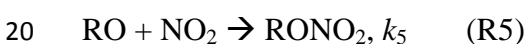
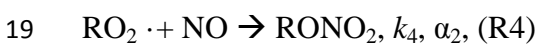
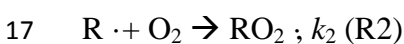
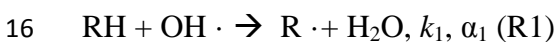
27 **Key word:** Alkyl nitrates; Source apportionment; Secondary formation; Biomass  
28 burning

29

## 1 **1. Introduction**

2 Alkyl nitrates (RONO<sub>2</sub>) are important photochemical pollutants in the atmosphere due  
3 to their roles in local, regional and global atmospheric chemistry (Jenkin et al., 2000;  
4 Seinfeld and Pandis, 2006). Alkyl nitrates are reactive nitrogen compounds (NO<sub>y</sub>) and  
5 act as a critical reservoir of nitrogen oxides (NO<sub>x</sub> = NO + NO<sub>2</sub>) during long-range  
6 transport due to their relatively low reactivity (Atkinson, 2006).

7 A number of studies conducted in different environments have shown that alkyl  
8 nitrates are either emitted from marine sources directly and/or produced indirectly  
9 through photochemical reactions (Roberts et al., 1998; Blake et al., 2003; Simpson et  
10 al., 2002, 2003, 2006; Reeves et al., 2007; Wang et al., 2013). In the case of biomass  
11 burning, secondary alkyl nitrate formation is believed to occur by the photo-oxidation  
12 of emitted hydrocarbons with a formation mechanism of RO and NO<sub>2</sub> (Simpson et al.,  
13 2002). The photochemical pathways for the secondary formation of alkyl nitrates are  
14 expressed as follows (Atkinson et al., 2006; Jenkin et al., 2000; Arey et al., 2001;  
15 Sommariva et al., 2008):

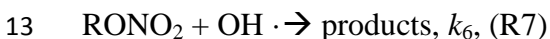


21 where  $k_1, k_2, k_3, k_4$  and  $k_5$  are reaction rate constants.  $\alpha_1$  and  $\alpha_2$  are branching ratios for  
22 the corresponding radicals, which increase as the carbon number increases and are  
23 dependent on the carbon chain length.

24 Photochemical formation of alkyl nitrates influences the oxidation of NO to NO<sub>2</sub>,  
25 subsequently leading to O<sub>3</sub> production by NO<sub>2</sub> photolysis. Therefore, alkyl nitrates are  
26 often used as indicators of photochemical O<sub>3</sub> production (Simpson et al., 2006).  
27 Furthermore, the interactions of alkyl nitrates with their parent hydrocarbons provide  
28 useful information about the photochemical processing of air masses. Comparing  
29 measured and predicted RONO<sub>2</sub>/RH ratios calculated using the laboratory kinetic data  
30 as a function of time, Bertman et al. (1995) examined the photochemical evolution of

1 alkyl nitrates at Scotia, Pennsylvania and the Kinterbish Wildlife Area, Alabama.  
2 Since then, this approach has been used to investigate the evolution of alkyl nitrates  
3 with air mass age in different regions (Simpson et al., 2006; Reeves et al., 2007;  
4 Russo et al., 2010; Worton et al., 2010; Wang et al., 2013). Fairly good agreement  
5 ( $>0.5$ ) between measured and modeled ratios suggests that the oxidation of  
6 single-parent hydrocarbons represents the evolution of their daughter alkyl nitrates,  
7 while poor correlation indicated sources other than photochemical formation of alkyl  
8 nitrates.

9 In contrast, the main sinks for ambient alkyl nitrates are photolysis and reactions with  
10 hydroxyl radical (OH), making alkyl nitrate lifetimes vary with season, latitude and  
11 altitude (days to weeks):



14 where  $h\nu$  is sunlight and  $J_{\text{RONO}_2}$  and  $k_6$  are the photolysis and OH reaction rate  
15 constants, respectively. The importance of alkyl nitrate removal by photolysis  
16 decreases as the carbon number increases (Clemmitshaw et al., 1997; Talukdar et al.,  
17 1997). Dry deposition has recently been recognized as another pathway for the  
18 removal of atmospheric alkyl nitrates (Russo et al., 2010; Wu et al., 2011).

19 Despite increased concern over photochemical pollution in Hong Kong and the  
20 greater Pearl River Delta (PRD) region, limited studies have focused on the  
21 characteristics of alkyl nitrates, which share a common mechanism with  
22 photochemical  $\text{O}_3$  formation and act as indicators of photochemical processing. For  
23 example, based on measurements conducted in 2001-2002, including during ozone  
24 episodes, Simpson et al. (2006) analyzed the general characteristics of alkyl nitrates at  
25 a coastal site (Tai O) in Hong Kong.  $\text{C}_3$ - $\text{C}_4$  alkyl nitrates were the most abundant  
26 species, with maximum and minimum levels in winter and summer, respectively. The  
27 diurnal variations suggested that photochemical production was the dominant source  
28 of alkyl nitrates at Tai O. Furthermore, through approximate calculations, it was  
29 concluded that the methoxy radical ( $\text{CH}_3\text{O} \cdot$ ) reaction with  $\text{NO}_2$  was a viable  
30 alternative pathway for the observed high levels of  $\text{MeONO}_2$  during pollution

1 episodes. This mechanism was subsequently verified by Archibald et al. (2007) via  
2 box model simulations, whereby  $\text{RO} + \text{NO}_2 \rightarrow \text{RONO}_2$  became important for  
3  $\text{MeONO}_2$  formation at 10 ppb  $\text{NO}_2$  and dominant at 35 ppb  $\text{NO}_2$ . However,  
4 knowledge related to the chemical evolution and source apportionments of individual  
5 alkyl nitrates and their relationship with parent hydrocarbons is still lacking in Hong  
6 Kong, especially given that levels of alkyl nitrate precursors have varied since 2002  
7 (Ling and Guo 2014). Hence, in this study, intensive field measurements of  $\text{C}_1\text{-C}_4$   
8 alkyl nitrates were conducted at two sites - a mountain site (Mt. Tai Mo Shan, TMS)  
9 and an urban site (Tsuen Wan, TW) at the foot of the same mountain in Hong Kong.  
10 The data were analyzed and compared with the previous study conducted at Tai O  
11 (Simpson et al., 2006). The aims were to investigate the spatiotemporal variations and,  
12 for the first time, source apportionments and photochemical formation pathways and  
13 evolution of alkyl nitrates in Hong Kong.

14

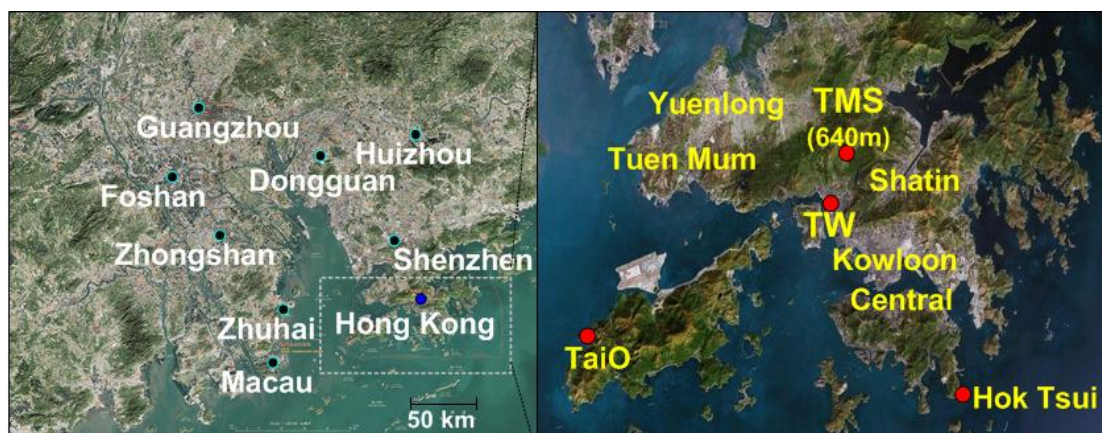
## 15 **2. Methodology**

### 16 **2.1. Sampling sites**

17 In this study, concurrent field measurements were conducted at two sites located at  
18 different elevations of the highest mountain, *i.e.*, Mt. Tai Mo Shan (TMS) with an  
19 elevation of 957 m a.s.l. in Hong Kong from September 6 to November 29, 2010. A  
20 detailed description of the topography of Mt. TMS was provided in an overview paper  
21 (Guo et al., 2013a). In brief, Figure 1 presents the two sampling locations and the  
22 surroundings. The high-elevation site (TMS) was set on the rooftop of a building on  
23 the mountainside (640 m a.s.l.), the highest logistically feasible observation location,  
24 beyond which the area comprised the natural landscape with shrubs and grasses to the  
25 mountain summit (AFCD, 2008). The measurement site at the foot of the mountain  
26 was the monitoring station of the Hong Kong Environmental Protection Department  
27 (HKEPD) at Tsuen Wan (TW), a mixed residential, commercial and light industrial  
28 area in the New Territories of Hong Kong. The TW monitoring site was located on the  
29 rooftop of a building, approximately 15-20 m above ground level. The linear distance  
30 between the TMS and TW sites was about 7 km and the difference in elevation

1 between the two sites was 630 m. In general, the solar radiation was comparable at the  
2 two sites, while the temperature was higher and the relative humidity and wind speed  
3 were lower at the TW site (Guo et al., 2013a). The winds at TMS were generally from  
4 the north with speeds ranging from 0.02 to 4 m s<sup>-1</sup>, and the winds at TW were  
5 predominantly from the southeast at speeds of 1-3 m s<sup>-1</sup> with easterly winds at night  
6 and southerly winds during the day. Due to its unique topography, the air at TMS was  
7 often influenced by the mountain-valley breezes and regional transport (Guo et al.,  
8 2013a). Based on the average wind speed of 1.9 m/s, air masses transported from  
9 upwind locations, on both local (~7 km) and regional scales (~20 km), took  
10 approximately 1-3 hours to arrive at the TMS site (Guo et al., 2012, 2013a).

11 The Tai O sampling station was a rural/coastal site located on the western coast of  
12 Lantau Island in southwestern Hong Kong (elevation, 80 m a.s.l.) (Figure 1). This site  
13 overlooks the Pearl River Estuary to the west and north, and the South China Sea to  
14 the south. It is 32 km away from the urban center to the east and about the same  
15 distance from Macau/Zhuhai to the west. Major man-made sources in the region are  
16 located to the east, north and southwest. Local emissions are small because of a sparse  
17 population and light traffic. Due to Asian Monsoon circulation, this site is frequently  
18 affected by polluted continental air masses from the highly industrialized PRD region  
19 of mainland China in cold seasons. A detailed description of the site is provided in  
20 Wang et al. (2003).



21  
22 Figure 1. Tai Mo Shan (TMS) and Tsuen Wan (TW) sampling sites and the  
23 surrounding environments in Hong Kong.  
24

## 2.2. Sampling and analysis of volatile organic compounds (VOCs)

Whole air samples were collected on 10 O<sub>3</sub> episode days and 10 non-O<sub>3</sub> episode days using evacuated 2-L stainless steel canisters. Each of the collected canister samples was integrated over a 60-min sampling period. A total of 384 samples were collected at the two sites. The O<sub>3</sub> episode days were selected as the days with the highest daytime hourly O<sub>3</sub> level at a regional scale (higher than 100 ppbv), which were based on weather forecasts and meteorological data analysis, and confirmed by the observed O<sub>3</sub> mixing ratios. During non-O<sub>3</sub> episode days, one-hour integrated samples were collected at 2-h intervals from 0700 to 1900 local time (LT) (7 samples per day). On O<sub>3</sub> episode days, one-hour integrated samples were collected from 0900 to 1600 LT at 1-h intervals with additional integrated samples collected at 1800, 2100, 0000, 0300 and 0700 LT (a total of 13 samples per day). After the campaign, the canister samples were sent to the University of California, Irvine (UCI) for chemical analysis. Other studies have provided detailed descriptions of the analytical system and the quality control, detection limits and analysis precision of the VOC samples (Simpson et al., 2006, 2010). In brief, the precision and detection limit of the alkyl nitrate measurements is 5% and 0.02 pptv, respectively. The calibration scale for the alkyl nitrate measurements changed in 2008, increasing by factors of 2.13, 1.81, 1.24 and 1.17 for the C<sub>1</sub>, C<sub>2</sub>, C<sub>3</sub> and C<sub>4</sub> alkyl nitrates, respectively (Simpson et al., 2011). In other words, the alkyl nitrates reported at Tai O by Simpson et al. (2006) were lower than the data reported here, and the Tai O data have been adjusted to the new calibration scale to allow direct comparison with this work. The Tai O sampling campaign was conducted from 24 August 2001 to 31 December 2002. Different from the air samples collected at TMS and TW, each whole-air sample at Tai O was collected for only 1-min, and was then analyzed at UCI. Intensive sampling from 0700-1900 LT was conducted every 2-h during the selected pollution episodes (17-19 October 2001, 29-30 August, 5-6 September, 9-11 and 25 October, 6-8 and 12 November 2002). Apart from the intensive sampling days, samples were taken either daily or every few days, typically in the midafternoon (Simpson et al., 2006).

## 2.3. Continuous measurements of O<sub>3</sub>, CO and NO-NO<sub>2</sub>-NO<sub>x</sub>

1 At TMS, online measurements of O<sub>3</sub>, CO and NO-NO<sub>2</sub>-NO<sub>x</sub> were made using  
2 commercial analyzers. Ozone was measured using a commercial UV photometric  
3 instrument (Advanced Pollution Instrumentation (API), model 400E) that has a  
4 detection limit of 0.6 ppbv. Carbon monoxide was measured with a gas filter  
5 correlation, nondispersive infrared analyzer (API, Model 300E) with a heated  
6 catalytic scrubber (as purchased) to convert CO to carbon dioxide (CO<sub>2</sub>) for baseline  
7 determination. The detection limit was 30 ppbv for a 2-min average. The 2σ precision  
8 was about 1% for a level of 500 ppbv (2-min average) and the overall uncertainty was  
9 estimated to be 10%. NO, NO<sub>2</sub> and NO<sub>x</sub> were detected with a chemiluminescence  
10 NO-NO<sub>2</sub>-NO<sub>x</sub> analyzer (API, Model 200E) that had a detection limit of 0.5 ppbv. The  
11 O<sub>3</sub> analyzer was calibrated by using a transfer standard (Thermo Environmental  
12 Instruments (TEI) 49PS), while the other analyzers were calibrated daily by analyzing  
13 scrubbed ambient air (TEI, Model 111) and a span gas mixture weekly with a NIST  
14 (National Institute of Standards and Technology) traceable standard which was diluted  
15 to representative mixing ratios using a dynamic calibrator (EnviroNics, Inc., Model  
16 6100). The Standard (Scott-Marrin, Inc.) contained 156.5 ppmv CO (±2%), 15.64  
17 ppmv SO<sub>2</sub> (±2%), and 15.55 ppmv NO (±2%). For the O<sub>3</sub>, CO, NO and NO<sub>x</sub>  
18 analyzers, a data logger (Environmental Systems Corporation Model 8816) was used  
19 to control the calibrations and to collect 1-minute data.

20 In addition to the above chemical measurements, several meteorological parameters,  
21 including wind speed and direction, temperature, relative humidity and solar radiation,  
22 were measured by the integrated sensor suite (Vantage Pro TM & Vantage Pro 2 Plus  
23 TM Weather Stations, Davis Instruments).

24 At TW, hourly O<sub>3</sub>, CO, NO-NO<sub>2</sub>-NO<sub>x</sub> and meteorological data were obtained from  
25 the HKEPD (<http://epic.epd.gov.hk/ca/uid/airdata>). The hourly data were derived by  
26 averaging 1-min data subsequently over the same time interval as the TMS data.  
27 Detailed information about the measurements, quality assurance and control protocols  
28 can be found in the HKEPD report (HKEPD, 2012). In addition, Table S1 in the  
29 supplementary information shows descriptive statistics of main non-methane  
30 hydrocarbons (NMHCs) and trace gases at both sites, while Figure S1 presents the



1 time series of trace gases and meteorological parameters at the two sites.

## 2 **2.4. Positive Matrix Factorization (PMF) model**

3 In this study, the US EPA PMF 3.0 (<http://www.epa/heads/products/pmf/pmf.html>)  
4 was used for the source apportionments of the observed alkyl nitrates at TW. Our  
5 previous studies provided detailed information about the PMF model (Ling et al.,  
6 2011; Ling and Guo, 2014). In terms of the PMF input, the uncertainty for each  
7 species was determined as the sum of 10% of the VOC concentration and two times  
8 the method detection limit (MDL) of the species (Paatero, 2000). Tracers for different  
9 sources were selected for the model input. For example, CO, ethane and ethyne were  
10 the tracers of combustion processes, and CH<sub>3</sub>Cl was specifically used for biomass  
11 burning. DMS was a typical tracer for marine emissions, while O<sub>x</sub> (*i.e.*, O<sub>3</sub> + NO<sub>2</sub>)  
12 was used as the tracer of secondary formation through photochemical reactions,  
13 including the formation of alkyl nitrates, because O<sub>3</sub> shares a common photochemical  
14 source with alkyl nitrates (Simpson et al., 2006). In addition to the aforementioned  
15 species, alkyl nitrate precursors, including methane, ethane, propane and *i/n*-butanes,  
16 were input into the model. In total, sixteen compounds were used for the model input.  
17 Various checks and sensitivity tests were conducted to examine the model  
18 performance. Firstly, many different starting seeds were tested and no multiple  
19 solutions were found. Secondly, the correlation between the predicted and measured  
20 concentration of each species was fairly good at TW ( $R^2=0.64\sim 0.94$ ) after the PMF  
21 implementation. Thirdly, the scale residuals, which are the uncertainty over the  
22 different runs for the input species, ranged between -3 and 3 for the PMF solution.  
23 Fourthly, the ratios of Q(robust)/Q(true) were close to 1 for 4-factor solution, within  
24 the ranges of 0.97-0.98 at TW, higher than those of 3-factor and 5-factor solutions,  
25 indicating all data points were fit better in the 4-factor solution. Indeed, the extracted  
26 source profiles from the 4-factor solution were the most reasonable. All the factors  
27 were mapped to a base factor in all the 100 runs in the bootstrapped simulation for the  
28 four-factor solution, suggesting the solution was stable. Lastly, the G-space plot  
29 extracted from the F-peak model results did not present oblique edges, reflecting that  
30 there was little rotation for the selected solution. Overall, the above features

1 demonstrated that PMF provided reasonable results for the source apportionment of  
2 alkyl nitrates (Ling et al., 2011; Ling and Guo, 2014).

### 3 **2.5. Photochemical box model incorporating master chemical mechanism** 4 **(PBM-MCM)**

5 A photochemical box model coupled with Master Chemical Mechanism (PBM-MCM)  
6 was used to simulate the in-situ formation of alkyl nitrates at TMS and TW. The  
7 PBM-MCM was developed by assuming that it was a well-mixed box without the  
8 treatment of vertical or horizontal dispersion, and the air pollutants in the model were  
9 homogeneous. For the mechanism coupled in the model, the MCM (version 3.2) used  
10 in this study is a state-of-the-art chemical mechanism, which describes the  
11 degradation of 143 primary VOCs including methane and contains around 16,500  
12 reactions involving 5900 chemical species (Jenkin et al., 1997, 2003; Saunders et al.,  
13 2003). The measured data, including O<sub>3</sub>, CO, NO<sub>x</sub>, SO<sub>2</sub>, 54 VOCs and methane,  
14 together with the actual meteorological conditions of temperature, relative humidity  
15 and boundary layer in the region, were used to constrain the model. The photolysis  
16 rates of different species in the model were parameterized as suggested by the  
17 previous study (Pinho et al., 2009) using the photon flux determined from the  
18 Tropospheric Ultraviolet and Visible Radiation (v5) model based on the actual  
19 conditions, such as meteorological conditions, location and time period of the field  
20 campaign in Hong Kong (Lam et al., 2013). The model output simulated in-situ  
21 formation of alkyl nitrates and other secondary products as well as the full set of  
22 precursors, radicals and intermediates. To provide robust results from the model  
23 simulation, several measures were adopted for the model development. The detailed  
24 information for the model frameworks, the model development and the evaluation for  
25 the model performance has been reported in our previous studies (Lam et al., 2013;  
26 Ling et al., 2014).

## 27 28 **3. Results and discussion**

### 29 **3.1 Descriptive statistics of alkyl nitrates and their parent hydrocarbons**

30 Table 1 presents the descriptive statistics of alkyl nitrates and their parent

1 hydrocarbons at TMS and TW. Figure 2 compares the levels of alkyl nitrates  
2 measured at TMS and TW with those measured in different environments in previous  
3 studies. In general, 2-PrONO<sub>2</sub> and 2-BuONO<sub>2</sub> were the most abundant alkyl nitrates  
4 at the two sites, consistent with the results observed in different environments (Blake  
5 et al., 2003; Simpson et al., 2006; Russo et al., 2010; Wang et al., 2013). The  
6 relatively higher levels of 2-PrONO<sub>2</sub> and 2-BuONO<sub>2</sub> were due to the balance between  
7 increased branching ratios for photochemical alkyl nitrate formation and the  
8 decreased lifetime of both parent alkanes and alkyl nitrates with increasing carbon  
9 number (Arey et al., 2001; Simpson et al., 2006; Russo et al., 2010). In comparison,  
10 the levels of MeONO<sub>2</sub>, EtONO<sub>2</sub> and 2-PrONO<sub>2</sub> were slightly higher at TW than at  
11 TMS ( $p < 0.05$ ), with average values of  $12.6 \pm 0.5$  (mean  $\pm$  95% confidence interval),  
12  $13.3 \pm 0.6$  and  $26.3 \pm 1.2$  pptv, respectively, at TW. The average mixing ratios of  
13 1-PrONO<sub>2</sub> and 2-BuONO<sub>2</sub> were comparable at the two sites ( $p > 0.05$ ). The results  
14 were contradictory to the fact that the mixing ratios of their parent hydrocarbons at  
15 TMS were much lower than at TW, highlighting the complexity of sources of alkyl  
16 nitrates at both sites.

17 In comparison with other studies, the average mixing ratios of alkyl nitrates at TMS  
18 were much higher than those measured in forested areas in coastal New England  
19 (Russo et al., 2010) and in tropospheric air influenced by Asian outflow during the  
20 airborne TRACE-P mission (Simpson et al., 2003), where the levels of parent  
21 hydrocarbons were also lower. (Note that all of the UCI data shown in Figure 2 were  
22 adjusted to UCI's post-2008 alkyl nitrates' calibration scale to enable direct  
23 comparison (Simpson et al., 2011). However, the mean mixing ratios of C<sub>1</sub>-C<sub>3</sub> alkyl  
24 nitrates were slightly lower and the 2-BuONO<sub>2</sub> mixing ratio was higher at TMS than  
25 at Tai O (Table 2), Hok Tsui and in Karachi, Pakistan (Barletta et al., 2002; the  
26 Karachi data have also been adjusted to the new UCI alkyl nitrates' calibration scale).  
27 The differences among TMS, Tai O and Hok Tsui might result not only from the  
28 levels of their parent hydrocarbons, but also from the influence of air masses with  
29 different photochemical ages and sources (Wang et al., 2003). Furthermore, as  
30 mentioned in Section 2.2, the sampling method and sampling period at TMS were

1 different from those at Tai O and Hok Tsui, where the sampling duration was only  
 2 1-min and the sampling time varied on different sampling days. In particular, many  
 3 whole air samples were collected during O<sub>3</sub> episodes at Tai O. These could also  
 4 induce differences in observed levels among the three sites. At the urban TW site, the  
 5 mean mixing ratios of alkyl nitrates were lower than those measured in urban areas in  
 6 Europe (Worton et al., 2010) and China (Wang et al., 2013). Compared to the average  
 7 values of alkyl nitrates at Tai O, the levels of EtONO<sub>2</sub>, 1-PrONO<sub>2</sub> and 2-BuONO<sub>2</sub>  
 8 were slightly higher and the MeONO<sub>2</sub> and 2-PrONO<sub>2</sub> mixing ratio was lower at TW.

9

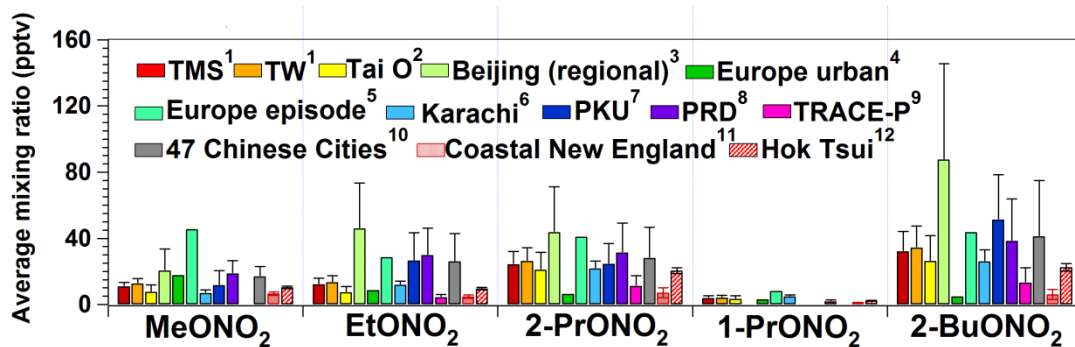
10 Table 1 Descriptive statistics of alkyl nitrates and parent hydrocarbons (pptv) in whole  
 11 air samples collected at TMS and TW during the sampling period.

Species	TMS			TW		
	Mean*	Min.	Max.	Mean	Min.	Max.
MeONO <sub>2</sub>	10.9±0.4	6.2	21.4	12.6±0.5	7.2	26.6
EtONO <sub>2</sub>	12.1±0.5	3.2	25.6	13.3±0.6	4.0	35.0
2-PrONO <sub>2</sub>	24.1±1.1	4.0	51.2	26.3±1.2	6.0	49.2
1-PrONO <sub>2</sub>	3.8±0.2	0.4	10.6	4.0±0.2	0.7	8.1
2-BuONO <sub>2</sub>	32.0±1.7	3.1	80.1	34.2±1.9	5.1	92.8
Methane (ppmv)	2.0±0.1	1.8	2.2	2.0±0.1	1.8	2.5
Ethane	1908±78	396	3588	2224±90	717	4315
Propane	1101±75	106	4455	3551±415	1443	33800
<i>n</i> -Butane	830±91	97	6252	4486±482	1372	34700

12 \* Average ± 95% confidence interval

13

14



15

16 Figure 2. Comparison of alkyl nitrate mixing ratios in different locations. Data  
 17 collected by UCI before 2008 (PRD and TRACE-P) were adjusted to UCI's new  
 18 calibration scale to permit direct comparison (see text for details about the new  
 19 calibration.

20 <sup>1</sup> This study, September-November, 2010. <sup>2</sup> Rural site, August 2001-December 2002 (Simpson et

1 al., 2006). <sup>3</sup> Urban site, 2009-2011 (Wang et al., 2013). <sup>4</sup> Urban sites, April-May 2004 (Worton et  
 2 a., 2010). <sup>5</sup> Urban sites, April-May 2004 (Worton et al., 2010). <sup>6</sup> Coastal site, December  
 3 1998-January 1999 (Barletta et al., 2002). <sup>7</sup> Urban site, August-September 2011 and December  
 4 2011-January 2012 (Wang et al., 2013). <sup>8</sup> Regional background sites, September 2009 (Wang et al.,  
 5 2013). <sup>9</sup> Aircraft measurement, February-April 2001 (Simpson et al., 2003). <sup>10</sup> Urban sites, July  
 6 2009 (Wang et al., 2013). <sup>11</sup> Coastal site, January-February and June-August 2002, July-August  
 7 2004 (Russo et al., 2010). <sup>12</sup> Regional background site, March 2001-April 2002 (unpublished  
 8 data).

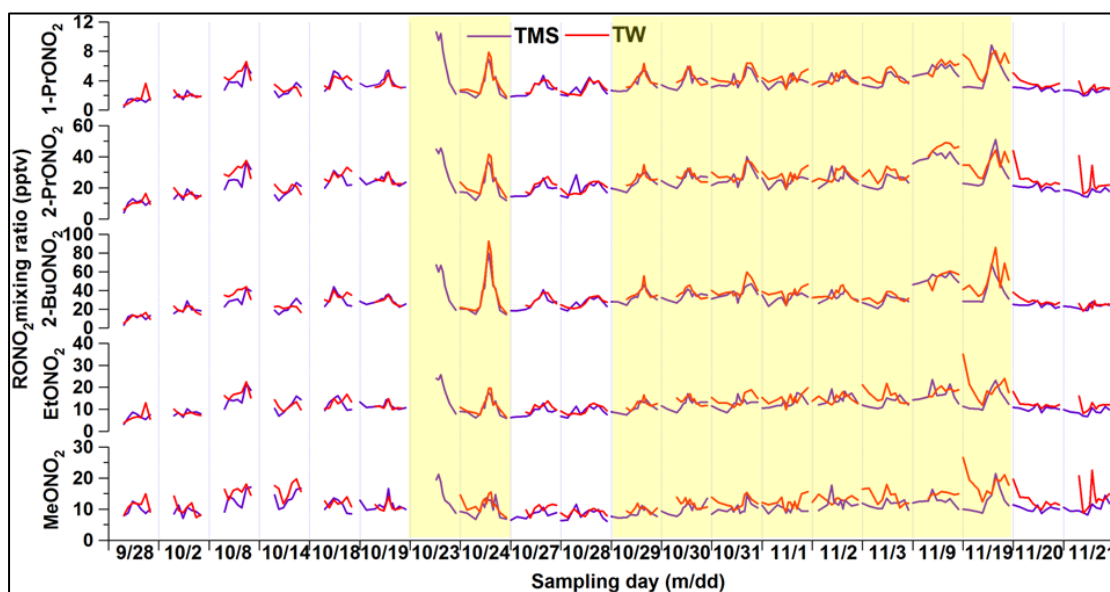
9  
 10  
 11 Table 2 Descriptive statistics of alkyl nitrate (pptv) and parent hydrocarbons (ppbv) in  
 12 whole air samples collected at Tai O between 24 August 2001 and 31 December 2002  
 13 (from Simpson et al., 2006).

Compound	Minimum	Maximum	Median	Mean
MeONO <sub>2</sub>	5.5	52.2	13.4	15.9
EtONO <sub>2</sub>	2.7	34.3	12.1	13.1
1-PrONO <sub>2</sub>	0.2	14.5	3.5	3.9
2-PrONO <sub>2</sub>	2.4	65.9	24.5	32.6
2-BuONO <sub>2</sub>	0.8	89.8	27.4	30.7
Methane (ppmv)	1.75	3.70	1.96	2.05
Ethane (ppbv)	0.38	5.05	2.14	2.12
Propane (ppbv)	0.006	13.0	1.54	2.05
<i>n</i> -Butane (ppbv)	0.006	12.8	0.95	1.64

14  
 15 Table S2 and Figure S2 in the supplementary information summarize the synoptic  
 16 weather conditions and the corresponding variations of O<sub>3</sub> and alkyl nitrates on O<sub>3</sub>  
 17 episode and non-O<sub>3</sub> episode days at both sites. In general, meteorological conditions  
 18 including temperatures, winds and solar radiation significantly influenced the levels  
 19 of air pollutants (Table S2). High mixing ratios of O<sub>3</sub> and alkyl nitrates were usually  
 20 associated with meteorological conditions with high-pressure system and/or stable  
 21 conditions, such as high temperatures, intense solar radiation and low wind speeds.  
 22 Figure 3 shows the time series of C<sub>1</sub>-C<sub>4</sub> alkyl nitrates on O<sub>3</sub> episode and non-O<sub>3</sub>  
 23 episode days at both sites, while Figure 4 presents the temporal variations of their  
 24 parent hydrocarbons accordingly. Although the ranges of alkyl nitrate mixing ratios  
 25 were similar and maximum values were observed in the afternoon, the day-to-day  
 26 variations of individual alkyl nitrates differed during the sampling period at both sites.  
 27 The maximum values were comparable and the diurnal patterns well tracked each

1 other for C<sub>3</sub>-C<sub>4</sub> alkyl nitrates at TMS and TW, especially on the days (24 October to 3  
2 November, 9 and 19 November) with relatively higher O<sub>3</sub> mixing ratios ( $p < 0.05$ ).  
3 The average daytime O<sub>3</sub> mixing ratios (0700-1800) on the high O<sub>3</sub> days were  $77 \pm 3$   
4 and  $38 \pm 3$  ppbv at TMS and TW, respectively, compared to  $58 \pm 3$  and  $23 \pm 3$  ppbv,  
5 respectively, on the non-O<sub>3</sub> episode days. Typically, the average daytime levels of  
6 2-PrONO<sub>2</sub>, 1-PrONO<sub>2</sub> and 2-BuONO<sub>2</sub> on high-level O<sub>3</sub> days at TMS were  $27 \pm 1$   
7 (TW:  $28 \pm 1$ ),  $4.5 \pm 0.3$  ( $4.4 \pm 0.2$ ) and  $37 \pm 2$  ( $39 \pm 3$ ) pptv, respectively, higher than  
8 those on non-O<sub>3</sub> episode days ( $p < 0.05$ ), implying that secondary formation of alkyl  
9 nitrates might be more prominent on O<sub>3</sub> episode days. Coincident with the high C<sub>3</sub>-C<sub>4</sub>  
10 alkyl nitrates during high O<sub>3</sub> days, their parent hydrocarbons, *i.e.*, propane (0.56-4.46  
11 and 1.55-10.4 ppbv for TMS and TW, respectively) and *n*-butane (0.28-6.25 and  
12 1.47-16.1 ppbv, respectively) also showed elevated mixing ratios (Figure 4), further  
13 suggesting an important source of C<sub>3</sub>-C<sub>4</sub> alkyl nitrates which was photo-oxidation of  
14 the parent hydrocarbons. For the C<sub>1</sub>-C<sub>2</sub> alkyl nitrates, the temporal patterns of  
15 MeONO<sub>2</sub> and EtONO<sub>2</sub> were different at the two sites, especially on high-level O<sub>3</sub>  
16 days. The peaks of MeONO<sub>2</sub> and EtONO<sub>2</sub> were usually observed between 11 a.m. and  
17 4 p.m. at TMS, except for 14 and 28 October, 1-2, 9, 20-21 November. The peaks of  
18 C<sub>1</sub>-C<sub>2</sub> alkyl nitrates corresponded to the high levels of methane and ethane observed  
19 at 11 a.m. to 5 p.m., likely indicative of photo-oxidation of methane and ethane, apart  
20 from potential influence of air masses in upwind areas due to regional transport (Guo  
21 et al., 2009; Jiang et al., 2010) and/or mesoscale circulations (Gao et al., 2005; Wang  
22 et al., 2006). At TW, however, besides the maximum concentrations observed in the  
23 afternoon, high levels of MeONO<sub>2</sub> and EtONO<sub>2</sub> were observed from midnight to early  
24 morning on 13 out of the 19 sampling days (*i.e.*, 2, 8, 14, 24, 28, 30-31 October, 1-3,  
25 19-21 November), when the prevailing winds switched to the southeast direction,  
26 implying that the high levels of MeONO<sub>2</sub> and EtONO<sub>2</sub> might be related to marine  
27 emissions and aged continental plumes which were re-circulated from the South  
28 China Sea to the coastal urban site at night. Indeed, this speculation was supported by  
29 the source apportionment results at TW, which confirmed that the high MeONO<sub>2</sub> and  
30 EtONO<sub>2</sub> levels from midnight to early morning on the above sampling days were

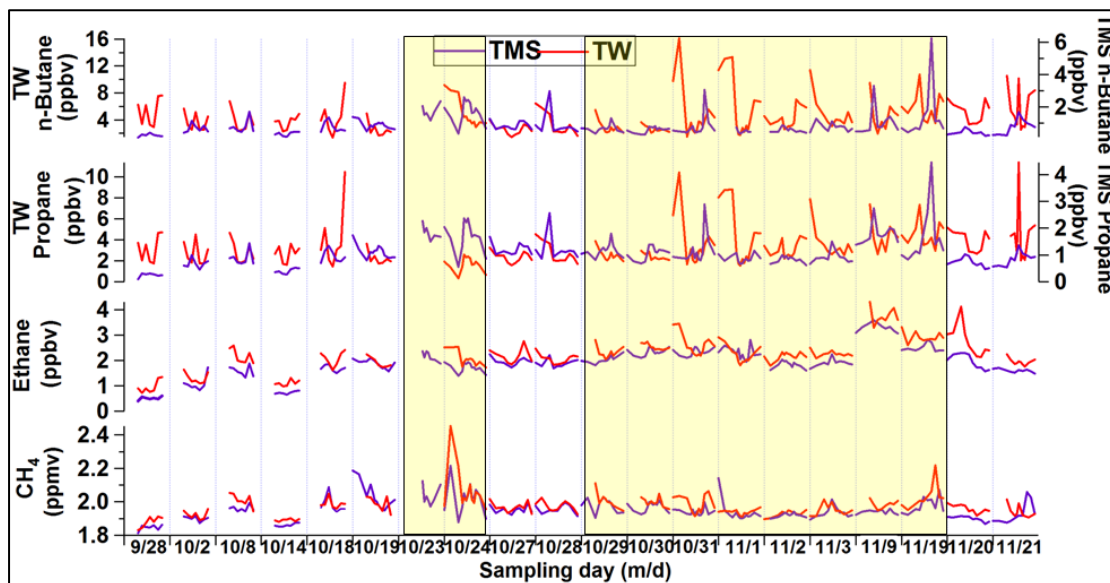
1 related to oceanic emissions (see Section 3.2.2 for details).



2

3 Figure 3. Time series of MeONO<sub>2</sub>, EtONO<sub>2</sub>, 1-PrONO<sub>2</sub>, 2-PrONO<sub>2</sub> and 2-BuONO<sub>2</sub>  
4 measured at TMS (purple) and TW (red) in 2010. The yellow shading highlights the  
5 O<sub>3</sub> episode days.

6



7

8 Figure 4. Time series of the parent hydrocarbons of alkyl nitrates at TMS and TW.  
9 The yellow shading highlights the O<sub>3</sub> episode days.

10

11 Although the levels of the parent hydrocarbons were lower at TMS, similar values of  
12 alkyl nitrates were observed at both sites, regardless of the elevation, suggesting the  
13 contributions of different sources and/or the influences of different air masses.  
14 Hence, the source apportionments of alkyl nitrates, contributions of reaction pathways

1 for the secondary formation of alkyl nitrates, and the relationship between O<sub>3</sub> and  
2 alkyl nitrates were analyzed in the following sections.

### 3 **3.2. Sources of alkyl nitrates**

#### 4 **3.2.1. Photochemical evolution of alkyl nitrates**

5 As photochemical oxidation of parent hydrocarbons is an important source of alkyl  
6 nitrates, it is helpful to study the photochemical evolution of alkyl nitrates. To do so,  
7 the relationships of alkyl nitrates with their parent hydrocarbons at the two sites were  
8 further examined using a simplified sequential reaction model developed by Bertman  
9 et al. (1995) (Equation 1), based on the assumptions that: (i) the hydrogen abstraction  
10 reaction from the parent hydrocarbon was the rate-limiting step for photochemical  
11 production of alkyl nitrates, and (ii) the reaction environment was NO<sub>x</sub>-rich, making  
12 the reaction with NO being the dominant pathway for the removal of RO<sub>2</sub> radicals  
13 (Russo et al., 2010). In this study, the average mixing ratios of NO<sub>x</sub> at TMS and TW  
14 were 10.7 ± 0.3 and 56.3 ± 1.6 ppbv, respectively, indicating that the environment was  
15 NO<sub>x</sub>-rich (> 0.1 ppbv, Roberts et al., 1998). Hence, reaction with NO was the main  
16 pathway for the removal of RO<sub>2</sub> radicals at the two sites. In addition, the results of  
17 PBM-MCM model simulation confirmed that the hydrogen abstraction reaction from  
18 the parent hydrocarbon, namely the reaction of hydrocarbon with OH radical, was  
19 indeed the rate-limiting step for photochemical production of alkyl nitrates at both  
20 sites (Lyu et al., 2015).

$$21 \quad \frac{RONO_2}{RH} = \frac{\beta k_A}{k_B - k_A} (1 - e^{(k_A - k_B)t}) + \frac{[RONO_2]_0}{[RH]_0} e^{(k_A - k_B)t} \quad (\text{Eq. 1})$$

22 where  $\beta = \alpha_1 \alpha_2$ ,  $k_A$  is the production rate for the formation of alkyl nitrates through the  
23 oxidation of hydrocarbons, RH ( $k_A = k_1[\text{OH}]$ ), while  $k_B$  is the destruction rate for alkyl  
24 nitrates through photolysis and the reaction with OH ( $k_B = k_5[\text{OH}] + J_{\text{RONO}_2}$ ).  
25  $[\text{RONO}_2]_0$  and  $[\text{RH}]_0$  are the initial concentrations of alkyl nitrates and the parent  
26 hydrocarbons before photochemical processing, respectively.  $[\text{OH}]$  is the diurnal  
27 average concentration of the OH radical. The relationships of alkyl nitrates with their  
28 parent hydrocarbons derived from the preceding equation are comparatively  
29 independent of the variations of OH and photolysis rates of alkyl nitrates (Roberts et

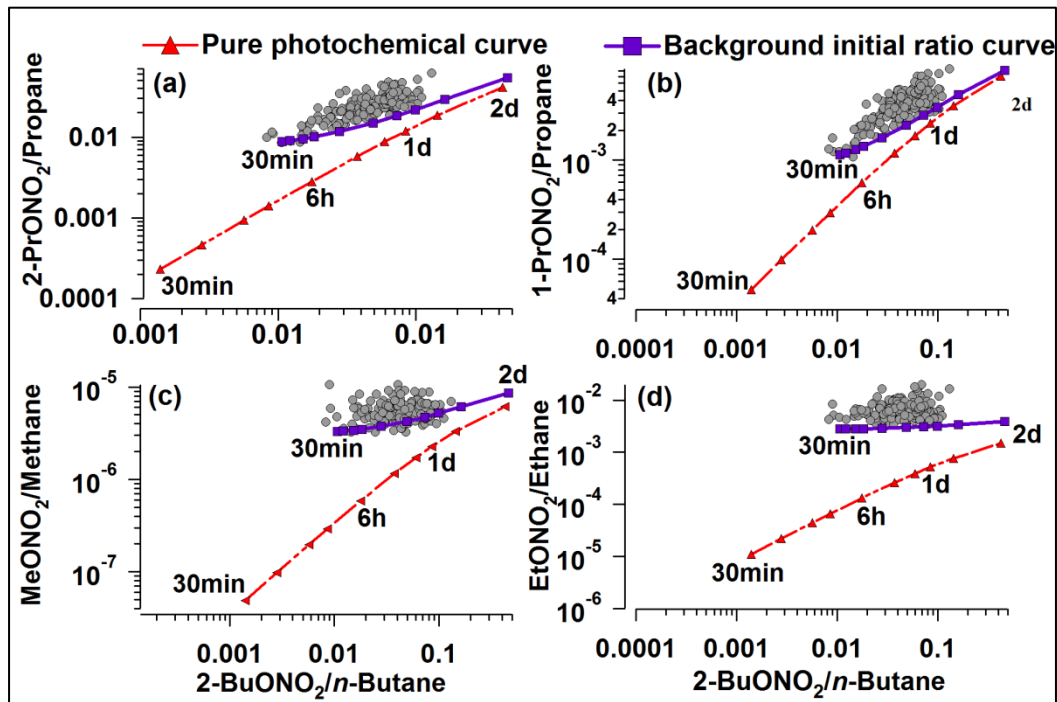


1 al., 1998; Wang et al., 2013). If the initial concentrations of alkyl nitrates and RH are  
2 zero, Equation 1 can be expressed as follows (Equation 2):

$$3 \quad \frac{RONO_2}{RH} = \frac{\beta k_A}{k_B - k_A} (1 - e^{(k_A - k_B)t}) \quad (2)$$

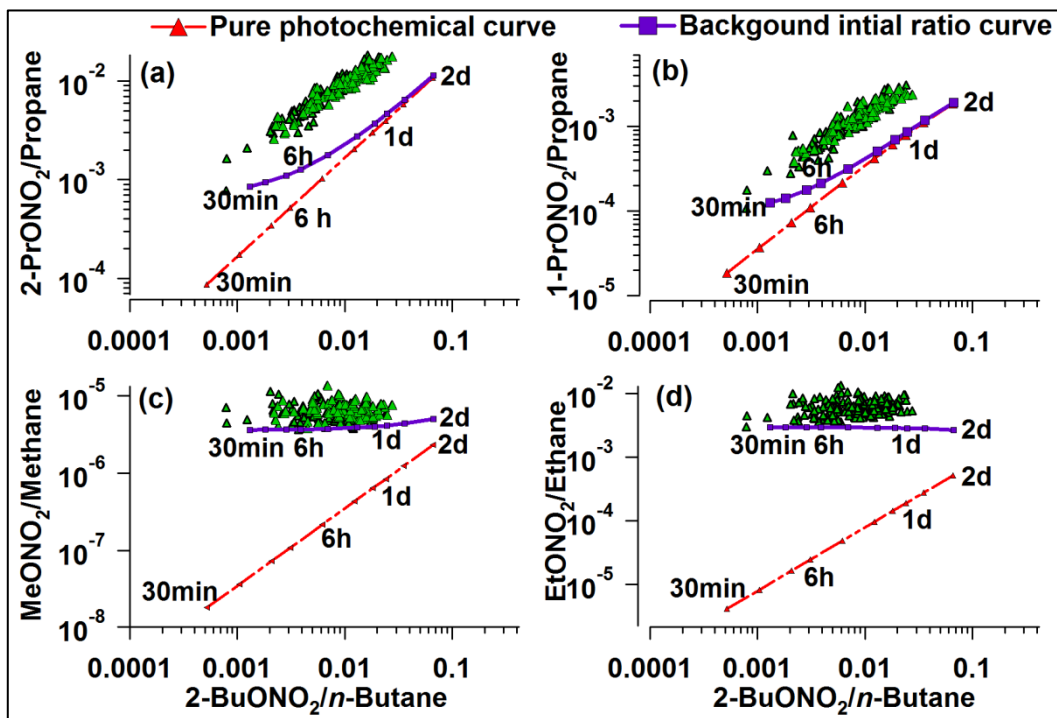
4 The relationships between alkyl nitrates and RH are obtained by plotting the measured  
5 ratios of  $RONO_2/RH$  to a specific ratio, 2-BuONO<sub>2</sub>/*n*-butane. The  
6 2-BuONO<sub>2</sub>/*n*-butane ratio has been widely used in the analysis of alkyl nitrates because  
7 *n*-butane is typically one of the most abundant hydrocarbons and 2-BuONO<sub>2</sub> is the  
8 most dominant alkyl nitrate (Roberts et al., 1998; Wang et al., 2013; Worton et al.,  
9 2010). Although some studies have investigated the relationships between alkyl  
10 nitrates and their parent hydrocarbons using zero initial values of alkyl nitrates, more  
11 recent studies have used non-zero initial values of alkyl nitrates to evaluate the  
12 influence of background levels on the photochemical evolution of alkyl nitrates  
13 (Reeves et al., 2007; Russo et al., 2010; Wang et al., 2013). Therefore, in addition to  
14 zero initial ratios, non-zero initial ratios of  $RONO_2/RH$ , equal to the lowest values  
15 from 0000 to 0700 measured at TMS and TW, respectively, as suggested by Wang et  
16 al. (2013), were used to investigate the relationships between alkyl nitrates and their  
17 parent hydrocarbons in this study. The diurnal average OH mixing ratios [OH] were  
18 simulated using the PBM-MCM (Lyu et al., 2016). By providing the values of  
19 photochemical processing time (*t*), the predicted ratios of  $RONO_2/RH$  were calculated  
20 since other parameters, *i.e.*,  $k_A$ ,  $k_B$ ,  $\alpha_1$ ,  $\alpha_2$  and  $J_{RONO_2}$  were obtained from literatures  
21 (Clemitchaw et al., 1997; Simpson et al., 2003; Worton et al., 2010; Wang et al., 2013).  
22 In this study, the given photochemical processing time ranged from 30 min to 2 days.  
23 The curves generated with zero initial values were the pure photochemical (PP)  
24 curves for the evolution of alkyl nitrates, and the curves with non-zero values, defined  
25 as background initial ratio (BIR) curves, were generated by assuming that both  
26 photochemical formation and background levels contributed to the distribution of  
27 alkyl nitrates (Russo et al., 2010; Wang et al., 2013). Consistent with previous studies  
28 (Russo et al., 2010; Wang et al., 2013), the shapes of the BIR curves were different  
29 from those of PP curves. The BIR curves of C<sub>1</sub>-C<sub>3</sub> alkyl nitrates at both sites were

1 positioned above their PP curves at shorter processing time ( $t < 1$  d) and converged  
 2 towards the PP curves at longer processing times ( $t = 1.5-2$  d) (Figure 5), resulting  
 3 from the decreased influence of the parameter  $\frac{[RONO_2]_0}{[RH]_0} e^{(k_A - k_B)t}$  on the difference  
 4 between the two curves as the photochemical age increased (Wang et al., 2013). This  
 5 feature was more pronounced for C<sub>3</sub>-C<sub>4</sub> alkyl nitrates at TW (Figure 6) because of the  
 6 lower values of  $[RONO_2]_0/[RH]_0$  resulting from the high mixing ratios of propane and  
 7 *n*-butane (Ling and Guo, 2014). Figure 5 presents the relationships of C<sub>1</sub>-C<sub>3</sub>  
 8  $RONO_2/RH$  to 2-BuONO<sub>2</sub>/*n*-butane at TMS. The red dashed curves are pure  
 9 photochemical curves, while the blue solid curves are BIR curves with the lowest  
 10 ratios of  $RONO_2/RH$  from 0000 to 0700 LT as the background initial ratio. Similarly,  
 11 Figure 6 shows the relationships of C<sub>1</sub>-C<sub>3</sub>  $RONO_2/RH$  to 2-BuONO<sub>2</sub>/*n*-butane at TW.



12  
 13 Figure 5. Relationships of C<sub>1</sub>-C<sub>3</sub>  $RONO_2/RH$  with 2-BuONO<sub>2</sub>/*n*-butane at TMS. The  
 14 red dashed curves were obtained based on zero initial concentrations of RH and alkyl  
 15 nitrates (pure photochemical curves, PP), while the blue solid curves were obtained  
 16 based on non-zero initial levels (background initial ratio curves, BIR), with the lowest  
 17 ratios of  $RONO_2/RH$  from 0000 to 0700 LT.

18



1

2 Figure 6. Relationships of C<sub>1</sub>-C<sub>3</sub> RONO<sub>2</sub>/RH with 2-BuONO<sub>2</sub>/*n*-butane at TW. The  
 3 red dashed curves were obtained based on zero initial concentrations of RH and alkyl  
 4 nitrates (pure photochemical curves, PP), while the blue solid curves were obtained  
 5 based on non-zero initial levels (background initial ratio curves, BIR), with the lowest  
 6 ratios of RONO<sub>2</sub>/RH from 0000 to 0700 LT.

7

8 At TMS, the measured ratios of MeONO<sub>2</sub>/methane and EtONO<sub>2</sub>/ethane to  
 9 2-BuONO<sub>2</sub>/*n*-butane were much higher than the ratios in the PP curves (Figure 5c &  
 10 d), with the observed ratios larger than their theoretical ratios by factors of 5-25. As  
 11 expected, the observed trends approached the PP curves at a longer processing time,  
 12 suggesting that the measured ratios of C<sub>1</sub>-C<sub>2</sub> RONO<sub>2</sub>/RH to 2-BuONO<sub>2</sub>/*n*-butane were  
 13 influenced by aged air masses due to long atmospheric lifetimes and slow  
 14 photochemical degradation rates of methane and ethane (Worton et al., 2010; Russo et  
 15 al., 2010). However, the difference between the measured ratios and the predicted  
 16 ratios of C<sub>1</sub>-C<sub>2</sub> RONO<sub>2</sub>/RH to 2-BuONO<sub>2</sub>/*n*-butane in BIR curves was comparatively  
 17 smaller, further confirming that there were other sources contributing to ambient  
 18 C<sub>1</sub>-C<sub>2</sub> alkyl nitrates besides photochemical formation, including the background levels  
 19 of C<sub>1</sub>-C<sub>2</sub> alkyl nitrates and their parent hydrocarbons (direct measurements of RH in  
 20 Table 1) (Wang et al., 2013). For example, the average MeONO<sub>2</sub> and EtONO<sub>2</sub> mixing

1 ratios at Hok Tsui, a PRD regional background site, were  $10.4 \pm 0.7$  and  $9.6 \pm 0.7$   
2 pptv (unpublished data, 2001-2002), respectively.

3 With regard to  $C_3$  alkyl nitrates, the measured ratios of 1- and 2-PrONO<sub>2</sub>/propane to  
4 2-BuONO<sub>2</sub>/*n*-butane were closer to the ratios of the BIR curve than those of the PP  
5 curve at TMS, further revealing the influence of background  $C_3$  alkyl nitrates and  
6 their parent hydrocarbons. However, the evolution of the measured ratios of  $C_3$   
7 RONO<sub>2</sub>/RH to 2-BuONO<sub>2</sub>/*n*-butane agreed well with the predicted ratios of BIR and PP  
8 curves at TMS, indicating that secondary formation from propane oxidation  
9 contributed significantly to the ambient  $C_3$  alkyl nitrates, including the background  $C_3$   
10 alkyl nitrates. Consistent with previous studies, the slopes of the observed ratios of  $C_3$   
11 RONO<sub>2</sub>/RH to 2-BuONO<sub>2</sub>/*n*-butane were different from those in the PP and BIR  
12 curves (Russo et al., 2010; Wang et al., 2013). For example, the slopes of the observed  
13 ratios of 1- and 2-PrONO<sub>2</sub>/propane to 2-BuONO<sub>2</sub>/*n*-butane were  $0.04 \pm 0.01$  and  $0.26$   
14  $\pm 0.02$ , respectively, while the slopes for the BIR curves were  $0.02 \pm 0.01$  (PP curve:  
15  $0.02 \pm 0.01$ ) and  $0.12 \pm 0.01$  ( $0.10 \pm 0.01$ ), respectively. This was reasonable due to  
16 the difference in the number of samples and distribution of data between the observed  
17 ratios and the ratios of PP and BIR curves, particularly when the observed ratios were  
18 higher than the theoretical ones due to significant influence of the background levels  
19 of alkyl nitrates and RH (Russo et al., 2010; Wang et al., 2013). Therefore, to further  
20 investigate the influence of secondary formation and background mixing ratios on  $C_3$   
21 alkyl nitrates at TMS, the ratio of 1-/2-PrONO<sub>2</sub> was examined. Previous studies  
22 reported that the theoretical ratio of 1-/2-PrONO<sub>2</sub> was the ratio between the yield for  
23 1-PrONO<sub>2</sub> and 2-PrONO<sub>2</sub> formation, which was equal to the ratio of  
24  $\beta_{1\text{-PrONO}_2}/\beta_{2\text{-PrONO}_2}$  (0.21) (Simpson et al., 2003; Wang et al., 2013). If photochemical  
25 production was the dominant source of 1-PrONO<sub>2</sub> and 2-PrONO<sub>2</sub>, the observed ratios  
26 should be close to the theoretical ones. Indeed, the slope of 1-PrONO<sub>2</sub> and 2-PrONO<sub>2</sub>  
27 at TMS was 0.19 ( $R^2 = 0.86$ ,  $p < 0.05$ ), close to the theoretical ratio (0.21), confirming  
28 that photochemical production from propane, including in-situ photochemical  
29 production and transport of photochemically-formed  $C_3$  alkyl nitrates in urban areas  
30 and/or during transit from urban areas to TMS, was the dominant source of ambient

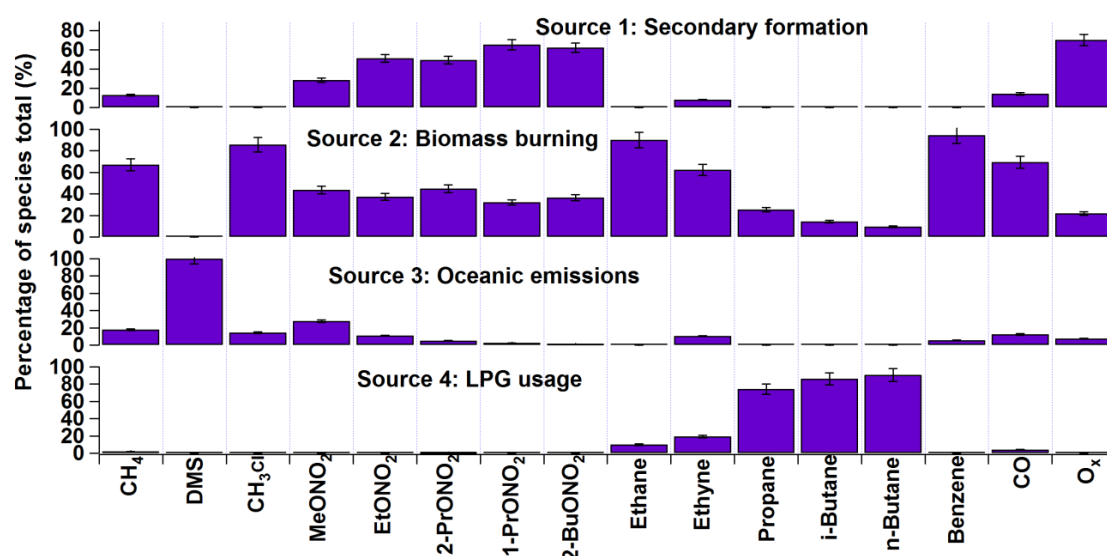
1 C<sub>3</sub> alkyl nitrates.

2 At TW, the comparison between the observed ratios of C<sub>1</sub>-C<sub>2</sub> RONO<sub>2</sub>/RH to  
3 2-BuONO<sub>2</sub>/*n*-butane and the ratios from the PP and BIR curves was consistent with  
4 that at TMS. However, in terms of C<sub>3</sub> alkyl nitrates, although the evolution of the  
5 measured ratios of C<sub>3</sub> RONO<sub>2</sub>/RH to 2-BuONO<sub>2</sub>/*n*-butane followed the trends of the  
6 ratios in the PP and BIR curves, the measured ratios of C<sub>3</sub> RONO<sub>2</sub>/RH to  
7 2-BuONO<sub>2</sub>/*n*-butane at TW were further away from the PP/BIR curves, about 2-3  
8 times the ratios in the PP and BIR curves, implying additional sources of C<sub>3</sub> alkyl  
9 nitrates (Wang et al., 2013) (details in Section 3.2.2). High emissions of propane  
10 provided sufficient precursors of C<sub>3</sub> alkyl nitrates, and the lifetimes of 1-PrONO<sub>2</sub> and  
11 2-PrONO<sub>2</sub> were long enough to sustain relatively high levels at TW. To further  
12 investigate the influence of additional sources on the distributions of C<sub>3</sub> alkyl nitrates  
13 at TW, equation 1 was used to fit the measured ratios of 1- and 2-PrONO<sub>2</sub>/propane to  
14 calculate the yield of C<sub>3</sub> alkyl nitrates ( $\beta$ ). The average yields of 1- and 2-PrONO<sub>2</sub>  
15 were  $0.032 \pm 0.004$  and  $0.22 \pm 0.02$ , respectively, higher than the laboratory kinetic  
16 values by factors of 4–9 (Kwok and Atkinson, 1995). This confirms the presence of  
17 additional emissions of C<sub>3</sub> alkyl nitrates at TW, including locally-emitted C<sub>3</sub> alkyl  
18 nitrates and/or secondary formation other than the production pathway from propane  
19 to proxyl radical and PrONO<sub>2</sub> (Reeves et al., 2007; Worton et al., 2010). The slope of  
20 1-PrONO<sub>2</sub> to 2-PrONO<sub>2</sub> at TW was 0.15 ( $R^2 = 0.80$ ,  $p < 0.05$ ), lower than the  
21 theoretical ratio of 0.21, further demonstrating the influence of other significant  
22 sources on ambient mixing ratios of C<sub>3</sub> alkyl nitrates at TW.

### 23 **3.2.2. Source apportionment of alkyl nitrates**

24 Figure 7 presents the explained variations of species (as a percentage of the species  
25 total) in the identified sources extracted by the PMF model. The standard errors in the  
26 figure were obtained from a bootstrap analysis of the PMF model simulation. Since  
27 the air masses arriving at TMS were photochemically aged (Guo et al., 2013a), the  
28 original source profiles of alkyl nitrates and their parent hydrocarbons were altered at  
29 this mountain site. Therefore, only the data collected at the urban site were used for  
30 source apportionments of alkyl nitrates.

1 High concentrations of O<sub>x</sub> and alkyl nitrates were found in the first factor at both sites,  
 2 implying that this factor was associated with secondary formation. In addition, certain  
 3 amounts of combustion species, such as ethane, ethyne, propane, *n/i*-butanes, benzene  
 4 and CO were present in this factor. It is not surprising that O<sub>x</sub> correlated with the  
 5 aforementioned species given that O<sub>3</sub> is a secondary pollutant formed from  
 6 photochemical oxidation of RH (Ling and Guo, 2014). The second factor was  
 7 distinguished by a significant presence of methyl chloride, ethene, ethyne and  
 8 benzene along with certain amounts of methane, propane and *n/i*-butane. It is well  
 9 established that methyl chloride, ethyne and benzene are typical tracers for biomass  
 10 burning/biofuel combustion (Barletta et al., 2009; Guo et al., 2011). As biofuel was  
 11 not in widespread use in Hong Kong (HKCSD, 2010), this factor was identified as  
 12 biomass burning. The third factor was identified as oceanic emissions, as the tracer  
 13 DMS had an exclusively high percentage in this source at both sites (Blake et al.,  
 14 2003; Marandino et al., 2013). The last factor was dominated by high percentages of  
 15 propane and *n/i*-butanes, typical tracers of liquefied petroleum gas (LPG). Therefore,  
 16 this factor was identified as LPG usage.



17  
 18 Figure 7. Explained variations of species in the identified sources extracted by the  
 19 PMF model for TW.

20  
 21 As mentioned earlier, regional transport and mesoscale circulation had a significant  
 22 influence on the distribution of air pollutants at TMS and TW (Guo et al., 2012,

1 2013a). By using the Weather Research and Forecasting (WRF) model, air masses  
2 affected by mesoscale circulation were distinguished from those affected by regional  
3 transport (Guo et al., 2013a). Nine sampling days during the entire sampling period  
4 (24, 29-31 October, 1-3, 9 and 19 November) were identified to be affected by  
5 mountain-valley breezes (they were also O<sub>3</sub> episode days). Hence, we divided the  
6 sampling period into two categories - “meso” and “non-meso” scenarios for source  
7 apportionment analysis. The “meso” scenario included the nine O<sub>3</sub> episode days with  
8 apparent mesoscale circulation, while the “non-meso” scenario covered the rest of the  
9 sampling days.

10 By summing up the mass of the alkyl nitrates in each source category, the overall  
11 mixing ratios in each source were obtained and the contribution of each individual  
12 source to alkyl nitrates at both sites was calculated. Figures 8 and 9 present the source  
13 contributions to individual alkyl nitrates for the “meso” and “non-meso” scenarios in  
14 percentage and in mixing ratio at TW, respectively. The mixing ratios of total alkyl  
15 nitrates (*i.e.*,  $\sum \text{RONO}_2 = \text{MeONO}_2 + \text{EtONO}_2 + 1\text{-PrONO}_2 + 2\text{-PrONO}_2 +$   
16  $2\text{-BuONO}_2$ ) were higher in the “meso” scenario than those in “non-meso” scenario ( $p$   
17  $< 0.05$ ), with the average value of  $100.9 \pm 7.5$  pptv for total alkyl nitrates in the “meso”  
18 scenario, about 1.4 times those in the “non-meso” scenario. It was found that in the  
19 “meso” scenario, secondary formation was the most significant contributor to the total  
20 alkyl nitrate mixing ratios, with an average percentage of  $60 \pm 2\%$  or absolute mixing  
21 ratio of  $60.2 \pm 1.2$  pptv, followed by biomass burning ( $34 \pm 1\%$  or  $35.1 \pm 0.4$  pptv)  
22 and oceanic emissions ( $6 \pm 1\%$  or  $5.62 \pm 0.06$  pptv). For the “non-meso” scenario, the  
23 contributions of biomass burning ( $46 \pm 2\%$  or  $34.2 \pm 0.7$  pptv) and secondary  
24 formation ( $44 \pm 2\%$  or  $32.9 \pm 0.7$  pptv) were comparable, and the oceanic emissions  
25 contributed  $10 \pm 1\%$  or  $7.0 \pm 0.07$  pptv to the total alkyl nitrates. The higher  
26 contribution of secondary formation in the “meso” scenario at TW was mainly due to  
27 higher degree of photochemical reactions. Indeed, the PBM-MCM model simulation  
28 indicated that the average concentration of HO<sub>x</sub> (HO<sub>x</sub> = OH + HO<sub>2</sub>) during daytime  
29 hours (0700-1800 LT) in the “meso” scenario was  $(2.5 \pm 0.7) \times 10^7$  molecule/cm<sup>3</sup>,  
30 about twice that of the “non-meso” scenario.

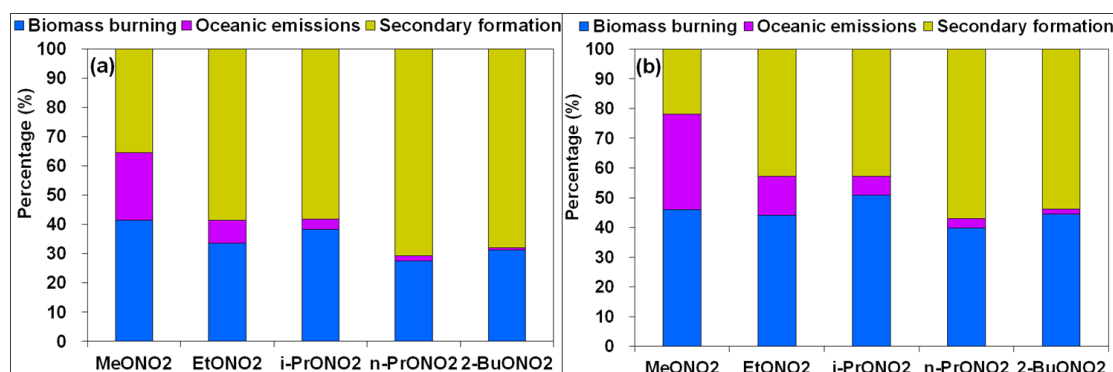


Figure 8. Source contributions to individual alkyl nitrates in (a) “meso” and (b) “non-meso” scenarios at TW (in percentage).

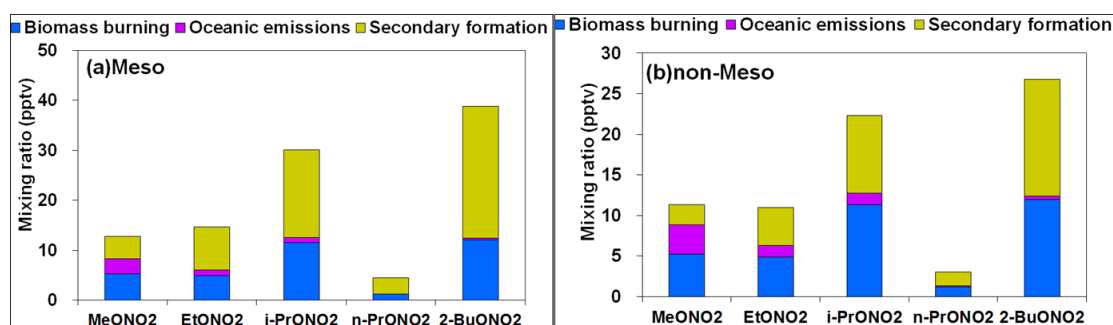


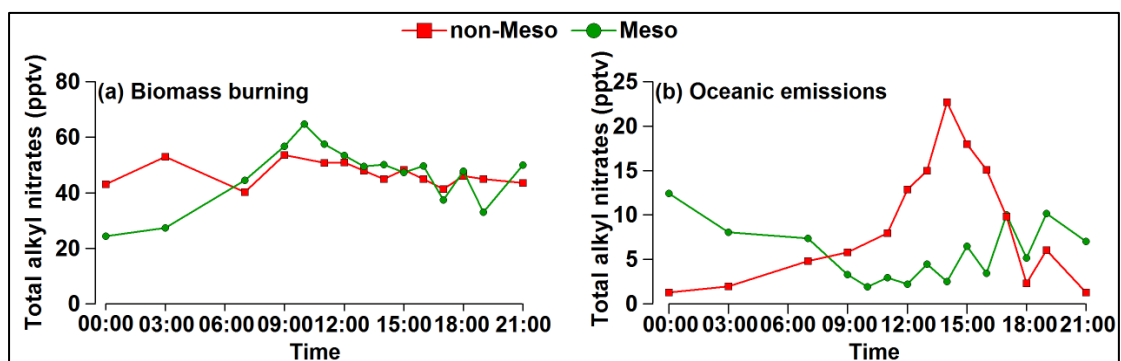
Figure 9. Source contributions to individual alkyl nitrates in (a) “meso” and (b) “non-meso” scenarios at TW (in summed mixing ratio).

In addition, although the percentage contribution of biomass burning was higher in the “non-meso” scenario, the absolute mixing ratios of biomass burning were comparable in the two scenarios. Figure 10 shows the diurnal patterns of  $\Sigma$ RONO<sub>2</sub> from biomass burning and oceanic emissions in “meso” and “non-meso” scenarios at TW. The contribution of biomass burning in the “meso” scenario was likely attributable to local emissions, including the cooking/heating activities in the small villages nearby and the frequent barbecue activities at the foot of the mountain (Guo et al., 2013a, b), as well as the forest fire observed in the mountainous areas (AFCD, 2015). The regular cooking/heating activities from 0700 to 1400 LT in many dim sum restaurants in the village likely resulted in the increased levels of biomass burning in the morning until noon. In contrast, the diurnal pattern in “non-meso” scenario was weak and the maximum values were not statistically different from the minimum values. The difference of the average mixing ratio of  $\Sigma$ RONO<sub>2</sub> between daytime and nighttime hours was only 1 pptv for biomass burning. The weak diurnal variations in



1 the “non-meso” scenario suggests that the contribution of fresh biomass burning  
 2 emissions was insignificant, revealing the influence of regional transport from the  
 3 PRD region. This speculation was confirmed by the analysis of 12-h backward  
 4 trajectories, which showed that air masses in the “non-meso” scenario were mainly  
 5 from the inland PRD region (not shown). It is noteworthy that although air masses  
 6 were more aged in the “non-meso” scenario, the levels of alkyl nitrates were  
 7 comparable to those in the “meso” scenario, highlighting the strong emissions of  
 8 biomass burning in the PRD region (Yuan et al., 2010).

9 For the oceanic emissions, a minimum mixing ratio during daytime hours was found  
 10 for  $\Sigma$ RONO<sub>2</sub> in the “meso” scenario, while a broad peak was present during daytime  
 11 hours in the “non-meso” scenario. The daytime minimum mixing ratio in the “meso”  
 12 scenario at TW was related to uplifted valley breezes that brought alkyl nitrates away  
 13 from TW to TMS, while the higher nighttime values were probably due to marine  
 14 emissions and aged continental plumes which were re-circulated from the South  
 15 China Sea to the coastal urban site at night. In contrast, the broad daytime peak in the  
 16 “non-meso” scenario was likely associated with higher daytime temperature and solar  
 17 radiation, leading to higher oceanic emissions that were transported from eastern  
 18 China and southern China coastal regions to the TW site.



19  
 20 Figure 10. Diurnal patterns of (a) biomass burning and (b) oceanic emissions for  
 21 “meso” and “non-meso” scenarios at TW.

22  
 23 Moreover, the contributions of oceanic emissions to C<sub>1</sub>-C<sub>2</sub> alkyl nitrates were higher  
 24 than C<sub>3</sub>-C<sub>4</sub> alkyl nitrates, with average percentages of 23% and 32% for the “meso”  
 25 and “non-meso” scenarios (Figures 8 and 9), suggesting the importance of oceanic  
 26 emissions to C<sub>1</sub>-C<sub>2</sub> alkyl nitrates, consistent with the results of previous work

1 (Simpson et al., 2003). Instead, the C<sub>3</sub>-C<sub>4</sub> alkyl nitrates were dominated by the  
2 secondary formation in the “meso” scenario (58-71%), while the contributions of  
3 biomass burning and secondary formation to C<sub>3</sub>-C<sub>4</sub> alkyl nitrates were comparable in  
4 the “non-meso” scenario.

5

### 6 **3.2.3. Contributions of mesoscale circulation, in-situ formation and regional** 7 **transport to alkyl nitrates at TMS**

8 Valley breezes brought freshly-emitted parent hydrocarbons and alkyl nitrates from  
9 the urban areas at the foot of the mountain (TW) to the mountain summit (TMS)  
10 during daytime hours, redistributing the ambient levels of alkyl nitrates at TMS (Guo  
11 et al., 2013a; Lam et al., 2013). Except for MeONO<sub>2</sub>, which had comparable levels in  
12 both “meso” and “non-meso” scenarios, the mixing ratios of daytime C<sub>2</sub>-C<sub>4</sub> alkyl  
13 nitrates were all higher in “meso” scenario than those in “non-meso” scenario ( $p <$   
14  $0.05$ ), with the average values of  $14.21 \pm 0.79$ ,  $28.73 \pm 1.70$ ,  $4.67 \pm 0.29$  and  $40.21 \pm 2.79$   
15 pptv for EtONO<sub>2</sub>, *i*-PrONO<sub>2</sub>, *n*-PrONO<sub>2</sub> and 2-BuONO<sub>2</sub>, respectively. To quantify the  
16 influence of mesoscale circulation on the mixing ratios of alkyl nitrates at TMS, a  
17 moving box model coupled with master chemical mechanism (Mbox) was applied to  
18 the data collected on the days influenced by mesoscale circulation (*i.e.*, “meso”  
19 scenario) (Guo et al., 2013a). The model was developed based on an idealized  
20 trajectory movement between TMS and TW sites, with air pollutants transported from  
21 TW to TMS through the valley breeze during daytime hours (0800-1700 LT) when  
22 photochemical formation of alkyl nitrates was occurring, and eventually contributed  
23 to the ambient levels of alkyl nitrates at TMS. As such, the model was only  
24 constrained with the observed daytime data at TW. On the other hand, the night-time  
25 downslope flow occurred due to the mountain breeze after sunset until the next  
26 morning, and TMS was set as the center of the box model, which was constrained by  
27 the data collected at TMS only for that period (Lam et al., 2013).

28 Table 3 presents the average concentrations of C<sub>1</sub>-C<sub>4</sub> alkyl nitrates simulated by the  
29 Mbox model at TMS, *i.e.*, the values under the “meso” scenario. It should be noted  
30 that the comparison was only made for daytime alkyl nitrates (0800-1700LT), when  
31 the valley breeze occurred. The average mixing ratios of MeONO<sub>2</sub>, EtONO<sub>2</sub>,

1 1-PrONO<sub>2</sub>, 2-PrONO<sub>2</sub> and 2-ButONO<sub>2</sub> at daytime hours estimated using the Mbox  
2 model were  $9.97 \pm 0.85$ ,  $7.38 \pm 0.44$ ,  $3.08 \pm 0.16$ ,  $18.7 \pm 0.77$  and  $34.7 \pm 3.14$  pptv,  
3 respectively, accounting for 86%, 52%, 66%, 65% and 86% of the observed values at  
4 TMS during the same period, respectively. The results demonstrated that when there  
5 was mesocale circulation, the levels of alkyl nitrates at TMS were dominated by the  
6 photo-oxidation of their parent hydrocarbons originated from the urban site TW, one  
7 possible reason leading to similar levels of alkyl nitrates at the two sites, though the  
8 values of their parent hydrocarbons were lower at TMS.

9 For the “non-meso” scenario, the simulated levels of in-situ formation of MeONO<sub>2</sub>,  
10 EtONO<sub>2</sub>, 1-PrONO<sub>2</sub>, 2-PrONO<sub>2</sub> and 2-BuONO<sub>2</sub> at TMS were  $3.61 \pm 0.48$ ,  $2.18 \pm 0.29$ ,  
11  $1.03 \pm 0.13$ ,  $3.68 \pm 0.45$  and  $10.9 \pm 1.31$  pptv, respectively, accounting for 18-42% of  
12 the observed C<sub>1</sub>-C<sub>4</sub> alkyl nitrates, indicating that other sources rather than local  
13 photochemical formation made significant contributions to ambient levels of alkyl  
14 nitrates. As stated earlier, TMS was a mountain site with sparse anthropogenic  
15 emissions nearby. However, the prevailing synoptic northerly winds in “non-meso”  
16 scenario suggested possible regional sources of alkyl nitrates from inland PRD region  
17 to the mountain site. The impact of regional transport on the variations of air  
18 pollutants at TMS for the days without mesoscale circulation, especially when the  
19 prevailing winds were from the north with high speeds, was corroborated in Guo et al.  
20 (2013a). By excluding the locally-formed alkyl nitrates from their overall levels, the  
21 contribution of regional sources to alkyl nitrates was determined for TMS. The  
22 regional source contributions to MeONO<sub>2</sub>, EtONO<sub>2</sub>, 1-PrONO<sub>2</sub>, 2-PrONO<sub>2</sub> and  
23 2-BuONO<sub>2</sub> were  $7.07 \pm 0.50$ ,  $8.44 \pm 0.62$ ,  $2.11 \pm 0.22$ ,  $16.86 \pm 1.17$ , and  $15.15 \pm 1.49$   
24 pptv, respectively, accounting for 58-82% of the alkyl nitrates at TMS. It is  
25 noteworthy that the regional alkyl nitrates included influences from all source  
26 categories (photochemical formation, biomass burning and oceanic emissions) in the  
27 inland PRD region.

28

29

30

1 Table 3. Mixing ratios of C<sub>1</sub>-C<sub>4</sub> alkyl nitrates influenced by mesoscale circulation  
 2 (“Meso”), in-situ formation and regional transport at TMS (unit: pptv).

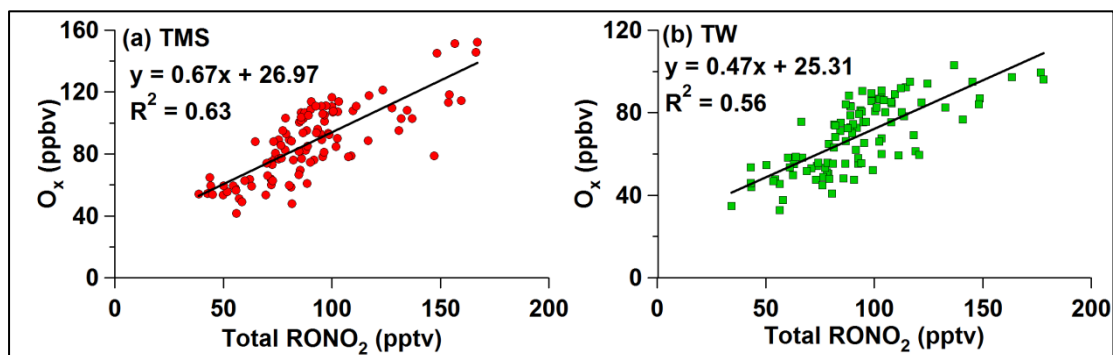
Scenario	MeONO <sub>2</sub>	EtONO <sub>2</sub>	1-PrONO <sub>2</sub>	2-PrONO <sub>2</sub>	2-BuONO <sub>2</sub>
“Meso”	9.97 ± 0.85	7.38 ± 0.44	3.08 ± 0.16	18.7 ± 0.77	34.7 ± 3.14
In-situ formation	3.61 ± 0.48	2.18 ± 0.29	1.03 ± 0.13	3.68 ± 0.45	10.9 ± 1.31
Regional transport	7.07 ± 0.50	8.44 ± 0.62	2.11 ± 0.22	16.86 ± 1.17	15.15 ± 1.49

3

### 4 **3.3. Relationship of alkyl nitrates with O<sub>3</sub>**

5 Alkyl nitrates are mainly formed through the reaction of peroxy radical (RO<sub>2</sub>) and NO.  
 6 However, NO can be oxidized by RO<sub>2</sub> to form NO<sub>2</sub>, which results in tropospheric O<sub>3</sub>  
 7 formation through NO<sub>2</sub> photolysis. Hence, investigating the relationship between  
 8 alkyl nitrates and O<sub>3</sub> is useful for evaluating the influence of alkyl nitrates on O<sub>3</sub>  
 9 formation (Simpson et al., 2006). Since photochemical formation of O<sub>3</sub> and alkyl  
 10 nitrates occurs during daytime hours, the relationship between O<sub>3</sub> and alkyl nitrates is  
 11 usually evaluated using the observed daytime data (*i.e.*, 0900-1600 LT). In this study,  
 12 the “oxidant” O<sub>x</sub> (O<sub>3</sub> + NO<sub>2</sub>) was considered to be a better representation of O<sub>3</sub> levels  
 13 as it takes into account the effect of O<sub>3</sub> titration by NO. Figure 11 shows the  
 14 correlation between O<sub>x</sub> and the total alkyl nitrates (ΣRONO<sub>2</sub>) at daytime hours. Good  
 15 correlations were found at TMS (R<sup>2</sup> = 0.63) and TW (R<sup>2</sup> = 0.56) with the slopes of  
 16 0.67 and 0.47 ppbv/pptv, respectively, suggesting that when 1 pptv of total alkyl  
 17 nitrates were formed from the reaction of RO<sub>2</sub> and NO, 0.67 and 0.47 ppbv of O<sub>x</sub>  
 18 could be simultaneously produced at TMS and TW, respectively. The relatively higher  
 19 slope at TMS than at TW was owing to higher concentrations of HO<sub>x</sub> radicals and  
 20 higher photochemical reactivity of VOCs at TMS (Lyu et al., 2016). In addition, as  
 21 the formation of alkyl nitrates consumes NO, it resulted in negative contribution to O<sub>3</sub>  
 22 formation. To quantify the negative influence on O<sub>3</sub>, the PBM-MCM model was  
 23 applied to the whole data collected at TMS and TW, respectively (Lyu et al., 2016).  
 24 The formation of alkyl nitrates made negative contributions to the O<sub>3</sub> production, with  
 25 the average reduction of 64.6 (TW: 24.9), 37.4 (11.0), 18.9 (2.6), 39.6 (11.1), and  
 26 115.1 (40.6) pptv of O<sub>3</sub> for the formation of MeONO<sub>2</sub>, EtONO<sub>2</sub>, 1-PrONO<sub>2</sub>,

1 2-PrONO<sub>2</sub> and 2-BuONO<sub>2</sub> at TMS, respectively. Furthermore, moderate to good  
2 correlation was found between the simulated O<sub>3</sub> reduction and the photochemically  
3 formed alkyl nitrates at TMS (R<sup>2</sup> = 0.42) and TW (R<sup>2</sup> = 0.72), with the average O<sub>3</sub>  
4 reduction rate of 4.1 and 4.7 pptv/pptv, respectively. Namely, O<sub>3</sub> was reduced by 4.1  
5 and 4.7 pptv if 1 pptv of alkyl nitrates were formed at TMS and TW, respectively.



6  
7 Figure 11. Correlation between O<sub>x</sub> (O<sub>3</sub> + NO<sub>2</sub>) and total alkyl nitrates at (a) TMS and  
8 (b) TW.

9  
10 Moreover, because secondary alkyl nitrates are formed through two main reaction  
11 pathways, “RO<sub>2</sub> + NO” and “RO + NO<sub>2</sub>”, it is of interest to investigate the relative  
12 contribution of the above pathways to the formation of alkyl nitrates. Two scenarios  
13 for model simulations were run and compared. The first scenario was the base case in  
14 which the model was run with all reaction pathways opened, while the second  
15 scenario was the constrained case in which the pathway of RO<sub>2</sub> + NO → RONO<sub>2</sub> was  
16 shut down. It was found that the reaction of “RO<sub>2</sub> + NO” was the prominent pathway  
17 for the secondary formation of alkyl nitrates at the two sites. The contributions of  
18 CH<sub>3</sub>O<sub>2</sub> + NO to MeONO<sub>2</sub> accounted for about 72% and 50% of the secondarily  
19 formed MeONO<sub>2</sub>, while the contributions of RO<sub>2</sub> + NO were 97-99 and 95-99% of  
20 the secondarily formed C<sub>2</sub>-C<sub>4</sub> alkyl nitrates at TMS and TW, respectively. The results  
21 are similar to the findings obtained at Tai O, Hong Kong (Lyu et al., 2015). The lower  
22 contributions of RO<sub>2</sub> + NO to MeONO<sub>2</sub> at the two sites were related to the higher  
23 levels of CH<sub>3</sub>O from the oxidation of CH<sub>4</sub> and the decomposition of larger RO<sub>2</sub>  
24 radicals.

25  
26

#### 1 **4. Conclusions**

2 Intensive field measurements of alkyl nitrates and their parent hydrocarbons were  
3 conducted concurrently at a mountain site (TMS) and an urban site (TW) at the foot  
4 of the same mountain in Hong Kong from September to November 2010. The levels  
5 of MeONO<sub>2</sub>, EtONO<sub>2</sub> and 2-PrONO<sub>2</sub> were slightly higher at TW than at TMS ( $p <$   
6  $0.05$ ), while the average mixing ratios of 1-PrONO<sub>2</sub> and 2-BuONO<sub>2</sub> were comparable  
7 at the two sites ( $p > 0.05$ ). However, the levels of the parent hydrocarbons of alkyl  
8 nitrates were lower at TMS, implying the complexity of sources of alkyl nitrates.  
9 Receptor model and photochemical box model simulations found that mesoscale  
10 circulation and regional transport had a significant impact on the levels of alkyl  
11 nitrates at the two sites. At TW, secondary formation was the dominant contributor to  
12 alkyl nitrates when there was mesoscale circulation, while the contributions of  
13 secondary formation and biomass burning were comparable under the influence of  
14 regional transport. At TMS, photo-oxidation of the parent hydrocarbons from TW  
15 contributed 52-85% to the ambient levels of alkyl nitrates on the days with mesoscale  
16 circulations between the two sites. On the other hand, alkyl nitrates from the inland  
17 PRD region were responsible for 58-82% of the observed values at TMS on the days  
18 with regional influence. The photo-oxidation of parent hydrocarbons from TW and  
19 regional transport led to the similar values of alkyl nitrates observed at the two sites.  
20 With regard to the secondarily formed alkyl nitrates, the reaction of RO<sub>2</sub> and NO was  
21 the prominent pathway at both sites. Moreover, the formation of alkyl nitrates made  
22 negative contributions to the O<sub>3</sub> formation, with a reduction rate of 4.1 and 4.7 pptv  
23 O<sub>3</sub> per pptv alkyl nitrates at TMS and TW, respectively. The findings of this study will  
24 aid in understanding the source contributions and photochemical formation pathways  
25 of alkyl nitrates in Hong Kong's mountainous areas.

#### 26 27 **Acknowledgements**

28 This project was supported by the Research Grants Council of the Hong Kong Special  
29 Administrative Region via grants PolyU5154/13E, PolyU152052/14E and  
30 CRF/C5022-14G. This study was partly supported by the internal grants of the Hong

1 Kong Polytechnic University (4-BCAV and 1-ZVCX), and the National Natural  
2 Science Foundation of China (No. 41405112 and 41275122). The challenging but  
3 ultimately very helpful comments of the anonymous reviewers are greatly  
4 appreciated.

## 5 **References**

- 6 AFCD (Agriculture, Fisheries and Conservation Department), 2008. Available at website:  
7 <http://www.afcd.gov.hk/>.
- 8 AFCD (Agriculture, Fisheries and Conservation Department), useful statistics, Last Review Date  
9 02 June 2015. Available at website: [http://www.afcd.gov.hk/english/country/cou\\_lea/  
10 cou\\_lea\\_use/cou\\_lea\\_use.html](http://www.afcd.gov.hk/english/country/cou_lea/cou_lea_use/cou_lea_use.html).
- 11 Archibald, A.T., Khan, M.A.H., Watson, L.A., Utembe, S.R., Shallcross, D.E., Clemmshaw, K.C.,  
12 Jenkin, M.E., 2007. Comment on 'Long-term atmospheric measurements of C<sub>1</sub>-C<sub>5</sub> alkyl  
13 nitrates in the Pearl River Delta region of southeast China' by Simpson et al. *Atmospheric  
14 Environment* 41, 7369-7370.
- 15 Arey, J., Aschmann, S.M., Kwok, E.S.C., Atkinson, R., 2001. Alkyl nitrate, hydroxyl nitrate, and  
16 hydroxycarbonyl formation from the NO<sub>x</sub>-air photooxidations of C<sub>5</sub>-C<sub>8</sub> n-alkanes. *Journal  
17 of Physical Chemistry* 105, 1020-1027.
- 18 Atkinson, R., Baulch, D.L., Cox, R.A., Crowley, J.N., Hampson, R.F., Hynes, R.G., Jenkin, M.E.,  
19 Rossi, M.J., Troe, J., Subcommittee, I., 2006. Evaluated kinetic and photochemical data for  
20 atmospheric chemistry: volume II – gas phase reactions of organic species. *Atmospheric  
21 Chemistry and Physics* 6, 3625-4055.
- 22 Barletta, B., Meinardi, S., Simpson, I.J., Atlas, E.L., Beyersdorf, A.J., Baker, A.K., Blake, N.J.,  
23 Yang, M., Midyett, J.R., Novak, B.J., Mckeachie, R.J., Fuelberg, H.E., Sachse, G.W., Avery,  
24 M.A., Campos, T., Weinheimer, A.J., Rowland, F.S., Blake, D.R., 2009. Characterization of  
25 volatile organic compounds (VOCs) in Asian and north American pollution plumes during  
26 INTEX-B: identification of specific Chinese air mass tracers. *Atmospheric Chemistry and  
27 Physics* 9, 5371-5388.
- 28 Barletta, B., Meinardi, S., Simpson, I.J., Khwaja, H.A., Blake, D.R., Rowland, F.S., 2002. Mixing  
29 ratios of volatile organic compounds (VOCs) in the atmosphere of Karachi, Pakistan.  
30 *Atmospheric Environment* 36, 3429-3443.
- 31 Bertman, S.B., Roberts, J.M., Parrish, D.D., Buhr, M.P., Goldan, P.D., Kuster, W.C., Fehsenfeld,  
32 F.C., Montzka, S.A., Westberg, H., 1995. Evolution of alkyl nitrates with air mass age.  
33 *Journal of Geophysical Research* 100, 22805-22813.
- 34 Blake, N.J., D. R. Blake, A. L. Swanson, E. Atlas, F. Flocke, and F. S. Rowland, 2003. Latitudinal,  
35 vertical, and seasonal variations of C<sub>1</sub>-C<sub>4</sub> alkyl nitrates in the troposphere over the Pacific  
36 Ocean during PEM-Tropics A and B: Oceanic and continental sources, *Journal of  
37 Geophysical Research* 108(D2), 8242, doi:10.1029/2001JD001444, 2003.

1 Clemitshaw, K.C., Williams, J., Rattigan, O.V., Shallcross, D.E., Law, K.S., Cox, R.A., 1997.  
2 Gas-phase ultraviolet absorption cross-sections and atmospheric lifetimes of several C<sub>2</sub>–C<sub>5</sub>  
3 alkyl nitrates. *Journal of Photochemistry and Photobiology A: Chemistry* 102, 117–126.

4 Gao, J., Wang, T., Ding, A.J., Liu, C.B., 2005. Observation study of ozone and carbon monoxide  
5 at the summit of mount Tai (1534 m a.s.l.) in central-eastern China. *Atmospheric*  
6 *Environment* 39, 4779-4791.

7 Guo, H., Jiang, F., Cheng, H.R., Simpson, I.J., Wang, X.M., Ding, A.J., Wang, T.J., Saunders, S.M.,  
8 Wang, T., Lam, S.H.M., Blake, D.R., Zhang, Y.L., Xie, M., 2009. Concurrent observations of  
9 air pollutants at two sites in the Pearl River Delta and the implication of regional transport.  
10 *Atmospheric Chemistry and Physics* 9, 7343-7360.

11 Guo, H., Cheng, H.R., Ling, Z.H., Louie, P.K.K., Ayoko, G.A., 2011. Which emission sources are  
12 responsible for the volatile organic compounds in the atmosphere of Pearl River Delta?  
13 *Journal of Hazardous Materials* 188, 116-124.

14 Guo, H., Ling, Z.H., Cheung, K., Jiang, F., Wang, D.W., Simpson, I.J., Barletta, B., Meinardi, S.,  
15 Wang, T.J., Wang, X.M., Saunders, S.M., Blake, D.R., 2013a. Characterization of  
16 photochemical pollution at different elevations in mountainous areas in Hong Kong.  
17 *Atmospheric Chemistry and Physics* 13, 3881-3898.

18 Guo, H., Ling, Z.H., Cheung, K., Wang, D.W., Simpson, I.J., Blake, D.R., 2013b. Acetone in the  
19 atmosphere of Hong Kong: Abundance, sources and photochemical precursors. *Atmospheric*  
20 *Environment* 65, 80-88.

21 Guo, H., Ling, Z.H., Simpson, I.J., Blake, D.R., Wang, D.W., 2012. Observations of isoprene,  
22 methacrolein (MAC) and methyl vinyl ketone (MVK) at a mountain site in Hong Kong.  
23 *Journal of Geophysical Research* 117, doi:10.1029/2012JD017750.

24 HKCSD (Hong Kong Census and Statistics Department), 2010. Hong Kong Energy Statistics:  
25 Annual Report. <http://www.censtatd.gov.hk>.

26 HKEPD (Hong Kong Protection Department), 2012. Air Quality in Hong Kong.  
27 2011. <http://www.epd-asg.gov.hk/english/report/aqr.html>.

28 Jenkin, M. E., Saunders, S. M., Wagner, V., and Pilling, M. J., 1997. The tropospheric degradation  
29 of volatile organic compounds: A protocol for mechanism development. *Atmospheric*  
30 *Environment* 31, 81-107, 1997.

31 Jenkin, M. E., Saunders, S. M., Wagner, V., and Pilling, M. J., 2003. Protocol for the development  
32 of the master chemical mechanism MCMv3 (Part B): Tropospheric degradation of aromatic  
33 volatile organic compounds, *Atmospheric Chemistry and Physics* 3, 181-193, 2003.

34 Jenkin, M.E., Clemitshaw, C., 2000. Ozone and other secondary photochemical pollutants:  
35 Chemical processes governing their formation in the planetary boundary layer. *Atmospheric*  
36 *Environment* 34, 2499-2527.

37 Jiang, F., Guo, H., Wang, T.J., Cheng, H.R., Wang, X.M., Simpson, I.J., Ding, A.J., Saunders, S.M.,  
38 Lam, S.H.M., Blake, D.R., 2010. An O<sub>3</sub> episode in the Pearl River Delta: field observation  
39 and model simulation. *Journal of Geophysical Research* 115, doi:/10.1029/2009JD013583.



1 Kwok, E.S.C. and Atkinson, R., 1995. Estimation of hydroxyl radical reaction-rate constants for  
2 gas-phase organic-compounds using a structure-reactivity relationship-an update.  
3 *Atmospheric Environment* 29, 1685-1695.

4 Lam, S.H.M., Saunders, S.M., Guo, H., Ling, Z.H., Jiang, F., Wang, X.M., Wang, T.J., 2013.  
5 Modelling VOC source impacts on high ozone episode days observed at a mountain summit  
6 in Hong Kong under the influence of mountain-valley breezes. *Atmospheric Environment* 81,  
7 166-176.

8 Lau, A. K.H., Yuan, Z.B., Yu, J.Z., Louie, P.K.K., 2010. Source apportionment of ambient volatile  
9 organic compounds in Hong Kong. *Science of the Total Environment* 408, 4138-4149.

10 Ling, Z.H. and Guo, H., 2014. Contribution of VOC sources to photochemical ozone formation  
11 and its control policy implication in Hong Kong. *Environmental Science and Policy* 38,  
12 180-191.

13 Ling, Z.H., Guo, H., Cheng, H.R., Yu, Y.F., 2011. Sources of ambient volatile organic compounds  
14 and their contributions to photochemical ozone formation at a site in the Pearl River Delta,  
15 southern China. *Environmental Pollution* 159, 2310-2319.

16 Ling, Z.H., Guo, H., Lam, S.H.M., Saunders, S.M., Wang, T., 2014. Atmospheric photochemical  
17 reactivity and ozone production at two sites in Hong Kong: Application of a Master Chemical  
18 Mechanism-photochemical box model. *Journal of Geophysical Research* 119,  
19 doi:10.1002/2014JD021794.

20 Lyu, X.P., Ling, Z.H., Guo, H., Zeng, L.W., Wang, N., 2016. Impact of alkyl nitrate chemistry on  
21 photochemical reactivity and O<sub>3</sub> production in Hong Kong. In preparation.

22 Lyu, X.P., Ling, Z.H., Guo, H., Saunders, S.M., Lam, S.H.M., Wang, N., Wang, Y., Liu, M., Wang,  
23 T., 2015. Re-examination of C<sub>1</sub>-C<sub>5</sub> alkyl nitrates in Hong Kong using an observation-based  
24 model. *Atmospheric Environment* 120, 28-37.

25 Marandino, C.A., Tegtmeier, S., Krüger, K., Zindler, C., Atlas, E.L., Moore, F., Bange, H.W., 2013.  
26 Dimethylsulphide (DMS) emissions from the western Pacific Ocean: a potential marine  
27 source for stratospheric sulphur? *Atmospheric Chemistry and Physics* 13, 8427-8437.

28 Paatero, P., 2000. User's guide for Positive Matrix Factorization Programs PMF2 and PMF3, part  
29 1: Tutorial. Prepared by University of Helsinki, Finland (February).

30 Pinho, P.G., Lemos, L.T., Pio, C.A., Evtugina, M.G., Nunes, T.V., Jenkin, M.E., 2009. Detailed  
31 chemical analysis of regional-scale air pollution in western Portugal using an adapted version  
32 of MCM v3.1. *Science of the Total Environment* 407, 2024-2038.

33 Reeves, C.E., Slemr, J., Oram, D.E., Worton, D., Penkett, S.A., Stewart, D.J., Purvis, R., Watson,  
34 N., Hopkins, J., Lewis, A., Methven, J., Blake, D.R., Atlas, E., 2007. Alkyl nitrates in outflow  
35 from North America over the North Atlantic during intercontinental transport of ozone and  
36 precursors 2004. *Journal of Geophysical Research* 112, D10S037, doi:  
37 10.1029/2006JD007567.

38 Roberts, J.M., Bertman, S.B., Parrish, D.D., Fehsenfeld, F.C., Johnson, B.T., Niki, H., 1998.  
39 Measurements of alkyl nitrates at Chebogue Point Nova Scotia during the 1993 North

1 Atlantic Regional Experiment (NARE) intensive. *Journal of Geophysical Research* 103 (D11),  
2 13569-13580.

3 Russo, R.S., Zhou, Y., Haase, K.B., Wingenter, O.W., Frinak, E.K., Mao, H., Talbot, R.W., Sive,  
4 B.C., 2010. Temporal variability, sources and sinks of C<sub>1</sub>-C<sub>5</sub> alkyl nitrates in coastal New  
5 England. *Atmospheric Chemistry and Physics* 10, 1865-1883.

6 Saunders, S. M., Jenkin, M. E., Derwent, R. G., and Pilling, M. J., 2003. Protocol for the  
7 development of the master chemical mechanism MCMv3 (Part A): Tropospheric degradation  
8 of non-aromatic volatile organic compounds. *Atmospheric Chemistry and Physics* 3,  
9 161-180.

10 Seinfeld, J.H. and Pandis, S.N., 2006. *Atmospheric Chemistry and Physics: from air pollution to*  
11 *climate change*, 2nd edition. Wiley Publisher, New Jersey, USA.

12 Simpson, I.J., Akagi, S.K., Barletta, B., Blake, N.J., Choi, Y., Diskin, G.S., Fried, A., Fuelberg,  
13 H.E., Meinardi, S., Rowland, F.S., Vay, S.A., Weinheimer, A.J., Wennberg, P.O., Wiebring, P.,  
14 Wisthaler, A., Yang, M., Yokelson, R.J., Blake, D.R., 2011. Boreal forest fire emissions in  
15 fresh Canadian smoke plumes: C<sub>1</sub>-C<sub>10</sub> volatile organic compounds (VOCs), CO<sub>2</sub>, CO, NO<sub>2</sub>,  
16 NO, HCN and CH<sub>3</sub>CN. *Atmospheric Chemistry and Physics* 11, 6445–6463.

17 Simpson, I.J., Blake, N.J., Barletta, B., Diskin, G.S., Fuelberg, H.E., Gorham, K., Huey, L.G.,  
18 Meinardi, S., Rowland, F.S., Vay, S.A., Weinheimer, A.J., Yang, M., Blake, D.R., 2010.  
19 Characterization of trace gases measured over Alberta oil sands mining operations: 76  
20 speciated C<sub>2</sub>-C<sub>10</sub> volatile organic compounds (VOCs), CO<sub>2</sub>, CH<sub>4</sub>, CO, NO, NO<sub>2</sub>, NO<sub>y</sub>, O<sub>3</sub> and  
21 SO<sub>2</sub>. *Atmospheric Chemistry and Physics* 10, 11931-11954.

22 Simpson, I.J., Blake, N.J., Blake, D.R., Atlas, E., Flocke, F., Crawford, J.H., Fuelberg, H.E., Kiley,  
23 C.M., Meinardi, S., Rowland, F.S., 2003. Photochemical production and evolution of selected  
24 C<sub>2</sub>-C<sub>5</sub> alkyl nitrates in tropospheric air influenced by Asia outflow. *Journal of Geophysical*  
25 *Research* 108, D20, doi:10.1029/2002JD002830.

26 Simpson, I.J., Meinardi, S., Blake, D.R., Blake, N.J., 2002. A biomass burning source of C<sub>1</sub>-C<sub>4</sub>  
27 alkyl nitrates. *Geophysical Research Letters* 29 (24), 2168, doi: 10.1029/2002GL016290.

28 Simpson, I.J., Wang, T., Guo, H., Kwok, Y.H., Flocke, F., Atlas, E., Meinardi, S., Rowland, F.S.,  
29 Blake, D.R., 2006. Long-term atmospheric measurements of C<sub>1</sub>-C<sub>5</sub> alkyl nitrates in the Pearl  
30 River Delta region of southeast China. *Atmospheric Environment* 40, 1619-1632.

31 Sommariva, R., Trainer, M., de Gouw, J.A., Roberts, J.M., Warneke, C., Atlas, E., Flocke, F.,  
32 Goldan, P.D., Kuster, W.C., Swanson, A.L., Fehsenfeld, F.C., 2008. A study of organic  
33 nitrates formation in an urban plume using a Master Chemical Mechanism. *Atmospheric*  
34 *Environment* 42, 5771-5786.

35 Talukdar, R.K., Burkholder, J.B., Hunter, M., Gilles, M.K., Roberts, J.M., Ravishankara, A.R.,  
36 1997. Atmospheric fate of several alkyl nitrates Part 2 UV absorption cross-sections and  
37 photodissociation quantum yields. *Journal of the Chemical Society, Faraday Transactions* 93,  
38 2797–2805.

39 Wang, M., Shao, M., Chen, W.T., Lu, S.H., Wang, C., Huang, D.K., Yuan, B., Zeng, L.M., Zhao,

1 Y., 2013. Measurements of C<sub>1</sub>-C<sub>4</sub> alkyl nitrates and their relationships with carbonyl  
2 compounds and O<sub>3</sub> in Chinese cities. *Atmospheric Environment* 81, 389-398.

3 Wang, T., Poon, C.N., Kwok, Y.H., Li, Y.S., 2003. Characterizing the temporal variability and  
4 emission patterns of pollution plumes in the Pearl River Delta of China. *Atmospheric*  
5 *Environment* 37, 3539-3550.

6 Wang, T., Wong, H.L.A., Tang, J., Ding, A., Wu, W.S., Zhang, X.C., 2006. On the origin of surface  
7 ozone and reactive nitrogen observed at a remote site in the northeastern Qinghai-Tibetan  
8 Plateau, western China. *Journal of Geophysical Research* 111, D08303, doi:  
9 10.1029/2005JD006527.

10 Worton, D.R., Reeves, C.E., Penkett, S.A., Sturges, W.T., Slemr, J., Oram, D.E., Bandy, B.J.,  
11 Bloss, W.J., Carslaw, N., Davey, J., Emmerson, K.M., Gravestock, T.J., Hamilton, J.F., Heard,  
12 D.E., Hopkins, J.R., Hulse, A., Ingram, T., Jacob, M.J., Lee, J.D., Leigh, R.J., Lewis, A.C.,  
13 Monks, P.S., Smith, S.C., 2010. Alkyl nitrate photochemistry during the tropospheric organic  
14 chemistry experiment. *Atmospheric Environment* 44, 773-785.

15 Wu, Z.Y., Wang, X.M., Chen, F., Turnipseed, A.A., Guenther, A., Niyogi, D., Charusombat, U.,  
16 Xia, B.C., Munger, J.W., Alapty, K., 2011. Evaluating the calculated dry deposition velocities  
17 of reactive nitrogen oxides and ozone from two community models over a temperate  
18 deciduous forest. *Atmospheric Environment* 45, 2633-2674.

19 Yuan, B., Liu, Y., Shao, M., Lu, S.H., Streets, D.G., 2010. Biomass burning contributions to  
20 ambient VOCs species at a receptor site in the Pearl River Delta (PRD), China.  
21 *Environmental Science and Technology* 44, 4577-4582.

22  
23  
24